Journal of Geophysical Research: Biogeosciences

RESEARCH ARTICLE
10.1029/2017JG004263

Key Points:
- A phytoplankton cell model describes allocation of gross photosynthate to balance cell demand for energy and reductant
- Cell functional pools are dynamically allocated, impacting elemental quotas
- A balance between iron, light, and oxygen determines the competitive balance for diazotrophic growth

Supporting Information:
- Supporting Information S1

Correspondence to:
D. P. Nicholson,
dnicholson@whoi.edu

Citation:
Nicholson, D. P., Stanley, R. H. R., & Doney, S. C. (2018). A phytoplankton model for the allocation of gross photosynthetic energy including the trade-offs of diazotrophy. *Journal of Geophysical Research: Biogeosciences*, *123*, 1796–1816. https://doi.org/10.1029/2017JG004263

Received 31 OCT 2017
Accepted 26 APR 2018
Accepted article online 1 MAY 2018
Published online 2 JUN 2018
Corrected 18 JUN 2018

This article was corrected on 18 JUN 2018. See the end of the full text for details.

A Phytoplankton Model for the Allocation of Gross Photosynthetic Energy Including the Trade-Offs of Diazotrophy

D. P. Nicholson[1], R. H. R. Stanley[2], and S. C. Doney[1,3]

[1]Marine Chemistry and Geochemistry Department, Woods Hole Oceanographic Institution, Woods Hole, MA, USA, [2]Department of Chemistry, Wellesley College, Wellesley, MA, USA, [3]Department of Environmental Sciences, University of Virginia, Charlottesville, VA, USA

Abstract Gross photosynthetic activity by phytoplankton is directed to linear and alternative electron pathways that generate ATP, reductant, and fix carbon. Ultimately less than half is directed to net growth. Here we present a phytoplankton cell allocation model that explicitly represents a number of cell metabolic processes and functional pools with the goal of evaluating ATP and reductant demands as a function of light, nitrate, iron, oxygen, and temperature for diazotrophic versus nondiazotrophic growth. We employ model analogues of *Synechoccocus* and *Crocosphaera watsonii*, to explore the trade-offs of diazotrophy over a range of environmental conditions. Model analogues are identical in construction, except for an iron quota associated with nitrogenase, an additional respiratory demand to remove oxygen in order to protect nitrogenase and an additional ATP demand to split dinitrogen. We find that these changes explain observed differences in growth rate and iron limitation between diazotrophs and nondiazotrophs. Oxygen removal imparted a significantly larger metabolic cost to diazotrophs than ATP demand for fixing nitrogen. Results suggest that diazotrophs devote a much smaller fraction of gross photosynthetic energy to growth than nondiazotrophs. The phytoplankton cell allocation model model provides a predictive framework for how photosynthate allocation varies with environmental conditions in order to balance cellular demands for ATP and reductant across phytoplankton functional groups.

1. Introduction

The growth of phytoplankton in the ocean depends on the photosynthetic production of energy (i.e., ATP) and reductant (e.g., NADPH). Photosynthetic activity and the use efficiency of these products is regulated by the availability of a host of resources in the ocean, including light, inorganic carbon, macronutrients, and trace elements that define a growth environment. Phytoplankton acclimate to a wide range of growth environments by adjusting their allocation of cellular resources and physiological activity. For example, culture studies show chlorophyll to carbon ratios varying from 3 to over 50 (mg chl/g C) over a range of light- and nitrogen-limited growth (Laws & Bannister, 1980). Much of this range has also been observed in field populations (Bouteiller et al., 2003; Landry et al., 2009; Li et al., 2010). Cellular C:N:P stoichiometry varies significantly depending on the nature of resource limitation (Geider & La Roche, 2002; Klausmeier et al., 2004). Altering cellular composition allows plankton to tune metabolism to best function under a given set of environmental conditions. From a modeling perspective, representing algal acclimation requires a dynamic approach, such that growth rate is a function not only of external environmental conditions (e.g., light, nutrients, and temperature) but also of cell status (e.g., chlorophyll content and internal nutrient stores; Geider et al., 1997, 1998).

Modeling phytoplankton is challenging, as the ocean contains an incredible diversity of photoautotrophic plankton, varying over orders of magnitude in size, displaying a wide range of morphology and adapted to a wide range of biomes. Despite this variety, phytoplankton rely on a common, core set of biochemical reactions for photosynthesis and growth, including the z-scheme of photosynthesis in photosystems I and II, carbon fixed by the Calvin cycle, catalyzed by ribulose-1,5-bisphosphate carboxylase oxygenase, (RuBisCO), catabolic and anabolic metabolism of fixed carbon, and the active uptake of nutrients from outside the cell. Each of these pathways is associated with certain organelles, or cellular functional pools, such as the light harvesting complex, nutrient transport proteins, or the biosynthetic apparatus, including ribosomes. This set of pathways and functional pools can serve as a common platform for a mechanistically based model for phytoplankton growth and acclimation.

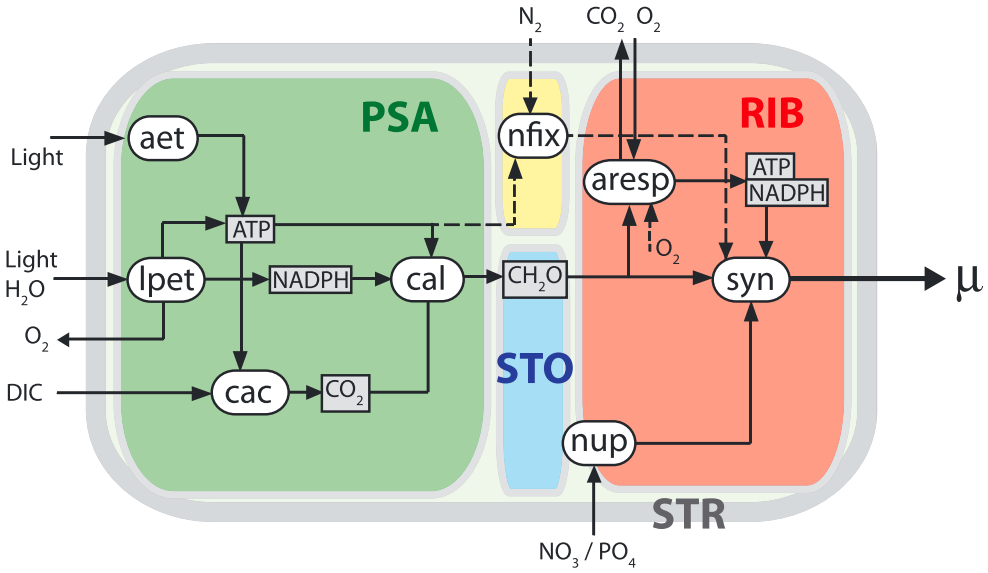

Figure 1. Schematic of the phytoplankton cell allocation model with metabolic pathways shown in white ovals and functional pools in colored segments. Pathways represented are linear photosynthetic electron transport (lpet), alternative electron transport (aet), carbon acquisition (cac), Calvin cycle fixation (cal), nitrogen fixation (nfix), nutrient uptake (nup), autotrophic respiration (aresp), and biosynthesis (syn). Functional pools are the photosynthetic apparatus (PSA; green), ribosomes and biosynthetic (RIB; red), nitrogenase (NIT; yellow), nutrient acquisition proteins (NAQ; blue), storage (STO; white), and structural cell wall (STR; gray). Black arrows indicate fluxes, with dashed lines denoting fluxes involved in diazotrophy.

Here we present a model framework for representing cellular-level strategies of phytoplankton energy allocation by explicitly representing the allocation of energy and resources amongst cellular functional pools. The fraction of gross photosynthetic activity that ultimately results in net growth is variable and generally less than 50% (Halsey & Jones, 2015). A dynamic representation linking gross photosynthesis to net C fixation is rarely included in phytoplankton models. In particular, we examine how the added trade-offs of diazotrophy, in which N requirements are met through biological reduction of N_2, alter such strategies depending on the environmental variables including iron, light, nitrogen, phosphorus, and oxygen. Our phytoplankton cellular allocation model (PCAM) is based on optimal allocation of cellular resources to maximize growth rate. We designed the model with the goal that it can, in the future, be applied both in Earth system models (ESMs) and in a diagnostic mode, using measured/observed environmental conditions to predict current phytoplankton state, such as photosynthetic rates and stoichiometry. Such applications would include estimating primary productivity from satellite models (satellite primary production model, SatPPM). In this initial implementation we focus on solving the model diagnostically for the balanced growth condition. The model can also run prognostically, and a future goal is incorporation into an ESM that would include full feedbacks of dynamic physics, chemistry, and biological top-down and bottom-up controls.

PCAM is designed to capture the fundamental physiological trade-offs of acclimation to multiple limiting nutrients, while retaining a minimal level of computational complexity so as to be appropriate for future integration into ESMs. PCAM (Figure 1) combines a number of theoretical principles previously explored in the literature. Each model cell consists of a number of interconnected functional pools (Shuter, 1979). Whole-cell C:N:P stoichiometry is flexible, varying with functional pool allocation (Flynn et al., 2001; Klausmeier et al., 2004; Pahlow & Oschlies, 2009). Nutrient uptake kinetics are dynamic and dependent on cell acclimation state. (Aksnes & Egge, 1991; Morel, 1987). Each cell has a fixed cell size and a number of cell physiological traits scale allometrically. (Litchman et al., 2007). Cells have variable cell Chl:C ratios (Geider et al., 1997). Furthermore, the model focuses on the distinctions between gross photosynthesis, gross carbon fixation, and net primary production (Halsey et al., 2010). The approach of optimal allocation to functional pools was pioneered by Shuter (1979) and recently has received renewed attention (Bruggeman & Kooijman, 2007; Clark et al., 2013; Daines et al., 2014; Pahlow & Oschlies, 2009, 2013; Smith et al., 2015; Talmy et al., 2013).

Here we present a similarly inspired model and apply trade-offs involved in diazotrophy as a competitive strategy for growth. Diazotrophy, a trait of a small number of organisms that are able to directly access dinitrogen gas as a nitrogen source, plays an important role in regulating the ocean nitrogen cycle and primary productivity (Galloway et al., 1995; Gruber & Sarmiento, 1997). Of critical importance to global biogeochemical cycling are feedbacks between nitrogen fixation and iron (Moore & Doney, 2007), as nitrogen fixers have high iron quota. Previous modeling work has investigated iron, light, and nitrogen colimitation (Armstrong, 1999), as well as the energetics and trade-offs of diazotrophy (Fernández-Castro et al., 2016; Pahlow et al., 2013; Rabouille et al., 2006, 2014). Here we apply an optimal allocation to explore the trade-offs of diazotrophy, in the context of varying iron and light availability.

In PCAM we apply a new mechanistic, optimal allocation model to explore explicitly the trade-offs of diazotrophy in the context of varying iron and light availability. In particular, we use the quantitative framework of the model to address how the unique energetic and metabolic demands of diazotrophic growth: (1) iron quota for nitrogenase, (2) respiratory cost for protecting nitrogenase from oxygen, and (3) energetic cost for nitrogen fixation affect strategies for the allocation of photosynthate by diazotrophs relative to nondiazotrophic organisms. Key metrics predicted from the model—photosynthetic use efficiency, growth rate, iron and light limitation, and relative fitness of diazotrophic versus nondiazotrophic growth of cyanobacteria—are compared against results from culture experiments and field measurements from a diversity of ocean biomes/biogeochemical provinces from six Joint Global Ocean Field Study (JGOFS) Process Study sites, from the California Cooperative Oceanic and Fisheries Investigation (CalCOFI), and from the GEOTRACES intermediate data product.

2. Model Description

PCAM (Figure 1) represents four core functional pools, the light harvesting complex (PSA), ribosomes and the biosynthetic apparatus (RIB), structural/cell wall (STR), and an internal storage pool for carbon (STO). A fifth pool for nitrogenase (NIT) is included for diazotrophs (Table 1). A core set of physiological pathways link internal cellular pools and the external environment. These include two photosynthetic pathways (linear photosynthetic electron transfer, lpet), and an alternative electron transfer pathway (aet), the calvin cycle (cal), uptake of inorganic N, P, and Fe (nup), nitrogen fixation for diazotrophs (nfix), and biosynthesis of new cells (syn). Autotrophic respiration (aresp) is also represented. Of the functional pools, carbon allocation to PSA, RIB, and STO is dynamically allocated based on a growth rate maximizing optimization.

2.1. Photosynthetic Pathways

On average, about 60% of gross photosynthetic electron flow is consumed by phytoplankton cell respiration with only 40% eventually allocated to cell growth (Halsey et al., 2012; Laws et al., 2000; Nicholson et al., 2012) and an even lower percentage results in net growth for diazotrophs (Großkopf & LaRoche, 2012; Kana, 1993). Thus, we argue that an explicit and flexible representation of pathways for energy and carbon allocation should be a central component of a mechanistic phytoplankton model.

The PSA pool is further divided to represent two photosynthetic pathways, lpet and aet, in order to represent variations in energy versus reductant requirement. Linear photosynthetic electron transport (lpet) produces reducing equivalents (NADPH) and energy (ATP) with the following stoichiometry (Allen, 2003; Baker et al., 2007; Geider et al., 2009):

$$2H_2O + 2NADP^+ + 2.6ADP + 2.6P_i + 8\ \text{photons} \xrightarrow{\text{yields}} 2NADPH + 2.6ATP + 4H^+ + O_2 \quad (1)$$

In our model, when allocation is optimal and growth balanced, lpet activity is stoichiometrically linked (1:1) with Calvin cycle (cal) fixing of inorganic carbon in order to achieve redox balance:

$$CO_2 + 2NADPH + 3ATP + 4H^+ \xrightarrow{\text{yields}} CH_2O + H_2O + 2NADP^+ + 3ADP + 3P_i \quad (2)$$

Additionally, in PCAM, 0.5 ATP is required for carbon acquisition (cac), effectively requiring 3.5 ATP per mol C fixed by cal (Raven et al., 2014). This approximate value of 0.5 was determined from averaging various estimated excess photon requirements for carbon concentration mechanisms (see Table 2, Raven et al., 2014) then applying the stoichiometry of equation (3) to convert to an ATP requirement of 0.45 ± 0.23 ATP per CO_2 fixed.

Table 1
Phytoplankton Cell Allocation Model Parameters and Variables

Symbol	Description	Value	Units	Source
r_{ref}	Reference cell radius	3×10^{-7}	m	–
r	Cell radius	prescribed	m	–
V	Cell volume	$V = 4\pi r^3/3$	m^3	–
C_{ref}	C per reference cell	4.09×10^{-15}	mol C per cel	Menden-Deuer and Lessard (2000)
γ	C:V power scaling	0.811	Unitless	Menden-Deuer and Lessard (2000)
C_m	C per cell	$C_{ref}(V/V_{ref})^{\gamma} \times 10^{-13}$	mol C per cell	–
ϕ^0_{STR}	Base structural allocation	0.2 C_m	mol C per cell	*
d	Cell wall thickness	1.0×10^{-7}	m	*
ϕ^w_{STR}	STR allocation for cell wall	Equation (8)	mol C per cell	–
ϕ_{STR}	Structural pool C	$(\phi^0_{STR} + \phi^w_{STR})C_m$	mol C per cell	–
ϕ_{PSA}	C allocation to PSA	Equation (S3-12)	mol C per cell	–
ϕ_{RIB}	C allocation to RIB	Equation (S3-10)	mol C per cell	–
ϕ_{STO}	Carbohydrate storage	Equation (16)	mol C per cell	–
R_0	Autotrophic respiration	0.5	Unitless	Halsey et al. (2010) and Halsey and Jones (2015)
R_{NFIX}	Respiratory demand for N-fixation	0.4 $[O_2]_{sat}$	Unitless	*
T_{func}	Eppley temperature function	$0.59e^{0.0633 \times T}$	Unitless	Eppley (1972)
a^{ref}_{syn}	Reference biosynthetic rate	10	mol C $[\text{mol C}]^{-1}$ /day	*
β	Metabolic rate V power scaling	0.75	Unitless	Brown et al. (2004)
a^m_{syn}	Maximum biosynthetic rate	Equation (7)	mol C $[\text{mol C}]^{-1}$/day	–
Photosynthesis variables and parameters				
α_{chl}	Initial slope of *P* versus *E* curve	3.0 μmol · rxn [g chl*a*] (μmol quanta) m^{-2}		*
χ_{chl}	Carbon to chlorophyll *a* ratio of PSA	1	mol C [g chl*a*]$^{-1}$	*
P^{ref}_{PSA}	Reference photosynthetic rate	22	mol rxn $[\text{mol C}]^{-1}$/day	*
P^m_{PSA}	Maximum photosynthetic rate	$P^{ref}_{PSA}(V/V_{ref})^{\gamma-\beta}$	mol rxn $[\text{mol C}]^{-1}$/day	–
E^*_k	Half saturation irradiance for gross photosynthesis	$\chi_{chl}P^m_{PSA}/\alpha_{chl}$	μmol quanta · m^{-2} · s^{-1}	–
E	PAR irradiance	Variable	μmol quanta · m^{-2} · s^{-1}	–
Nutrient variables and parameters				
V^S	Nutrient uptake rate	Equation (9)	mol *S*/s per cell	–
f^S_{Aup}	Max fraction of cell surface for uptake	2×10^{-3}	Unitless	*
A	Area of a transporter site	$\pi \times 10^{-18}$	m^2	*
n	Moles of uptake sites per cell	Equation (S1-8)	mol sites per cell	–
n_{max}	Maximum moles of uptake sites per cell	$4\pi r^2 f^S_{Aup}/A$	mol sites per cell	–
h	handling time per mol of ions	6.022×10^{21}	s/mol	*
D^S	T-dependent molecular diffusivity of *S*	Variable	m^2/s	Yuan-Hui and Gregory (1974)
K^S	[S] at which $V^S$is half of V^S_{max}	1/(Akh)	mol/m^3	–
K^S_{μ}	[S] at which μ is half of μ_{max}	Variable: see equation (12)	mol/m^3	–
Q^S	Cell quota	Variable: see equation (S3)	mol *S* per cell	–
Q^S_N	Quota of "*S*" for pool "*N*"	$\phi_N r^S_N$: see Table 2	mol *S* per cell	–
Nitrogen fixation variables and parameters				
R_{nfix}	Respiratory demand for N-fixation	0.4 $[O_2]_{sat}$	Unitless	Großkopf and LaRoche (2012)
r^{Fe}_{nfix}	Nitrogenase Fe content	0.2×10^{-5}	mol Fe/mol N	*
v^{Fe}_{nfix}	Nitrogen fixation rate	Variable	mol N/day	–

Note. The source for each model parameter and variable is designated by "asterisk" for this study, "en dash" indicates values derived from other variables/parameters.

Table 2
Elemental Stoichiometries for PCAM Functional Pools

Pool	C:N (mol:mol)	C:P (mol:mol)	C:Fe (mol:mol)
PSA (aet and lpet)	6.6	518	1.0×10^4
RIB	6.6	49	8.3×10^4
STR	6.6	106	8.3×10^4

Note. The STO pool contains only carbon and the NFIX pool contains only iron. PCAM = phytoplankton cell allocation model.

Given the imbalance in ATP production by lpet and demand from cal, an additional source of ATP is needed. The additional ATP is derived from a collection of alternative electron pathways that are not linked to carbon fixation including the Mehler cycle, midstream and terminal oxidase activity, cyclic photosynthetic electron transport, photorespiration, and the malate valve. While the activities of these individual pathways are not well constrained across functional types and environmental conditions, they serve a similar role in generating additional ATP. In PCAM, we model this host of processes with a representative aet pathway:

$$2H_2O + 3.4ADP + 3.4P_i + 8\ photons + O_2 \overset{yields}{\rightarrow} O_2 + 3.4ATP + 2H_2O \quad (3)$$

The aet pathway has the net effect of producing 3.4 ATP (Geider et al., 2009) without altering the cellular redox balance. Pathways such as the Mehler reaction photosynthetically produce O_2 originating from water molecules but also consume dissolved O_2. For each pathway (lpet and aet), a reaction requires 8 photons.

Total gross photosynthesis (G_{O2}) is thus lpet + aet, while gross carbon photosynthesis (G_C) is equal to lpet (also = cal). The distinction between G_{O2} and G_C is important when comparing to field and laboratory tracers, as techniques such as the triple oxygen isotope method (Luz & Barkan, 2000) and ^{18}O labeling measure G_{O2} while short-term radiocarbon methods (20 min–2 hr) most closely measure G_C. Based on the stoichiometry of ATP demand/yield of cal, aet, and lpet, 20% of G_{O2} is due to the aet reactions and 80% to lpet for nondiazotrophic growth, because an additional 0.9 ATP must be generated via aet for each C fixed by lpet. Condensing all ATP-generating pathways to the single aet pathway in PCAM omits the complexity of a range of pathways that to date have not been fully characterized. However, our result does agree well with a constant value of 19–22% measured for a diatom (*Thalassiosira weissflogii*), a chlorophyte (*Dunaliella tertiolecta*), and a prasinophyte (*Ostreococcus tauri*) across a range of nitrate-limited conditions (Halsey et al., 2013, 2014), and 20% measured for a nutrient replete *Synechococcus sp*. WH7803 (Kana, 1992). These studies suggest that while there may be differences in the pathways used for ATP generation, the requirement of about 20% supplementary ATP generation for carbon fixation appears robust.

A number of recognized photosynthetic processes are not represented in the version of PCAM presented here, including photoinhibition (Jassby & Platt, 1976; Platt et al., 1980) and the packaging effect (Morel & Bricaud, 1981). While these processes could be added in future versions, they are processes less relevant to acclimated phytoplankton under light limitation. Photoinhibition is much more significant for phytoplankton exposed to light levels differing greatly from their acclimated state (Anning et al., 2000), whereas in acclimated field populations in high light environments, photoinhibition is often not observed (Li et al., 2011). The packaging effect causes a reduction in chlorophyll a specific absorption relative to absorption in free water due to the physical packaging of chlorophyll in a cell geometry. It has a greater impact for larger cell sized with low surface area to volume ratios and at higher pigment concentrations and is lesser in the small cell sizes that are the focus of this manuscript (Bricaud et al., 2004).

2.2. Respiration and Biosynthesis

Carbon fixed by cal enters STO for subsequent use in anabolic and catabolic reactions. Of total G_C entering STO, we prescribe that 50% is consumed by autotrophic carbon respiration and the oxidative pentose phosphate pathway to produce the ATP and reducing equivalents needed for biosynthesis (Halsey & Jones, 2015). In the model, these two pathways are lumped together in a single autotrophic respiration pathway (aresp). Recent culture studies have shown that 50% of G_C is consumed by autotrophic respiration, and this fraction is relatively constant across nitrate-limited growth rates and across diverse taxa of nondiazotrophs (Halsey et al., 2010, 2012). The remaining 50% of G_C is retained for net growth N_C. Overall, our model N_C:G_{O2} is 0.4 for nondiazotrophic growth that is in good agreement with N_C:G_{O2} derived from field observations (Bender et al., 2000; Marra, 2002; Nicholson et al., 2012) and culture work (Halsey et al., 2013; Halsey & Jones, 2015), but somewhat lower than recent results for light-limited diatoms (Fisher & Halsey, 2016) and higher than has been observed in some cyanobacteria (Felcmanová et al., 2017; Kunath et al., 2012). The RIB pool is responsible for biosynthesis of new cells via the syn pathway, which uses the remaining N_C along with nutrients to create new cells.

2.3. Pathway Efficiencies

Photosynthetic efficiency in PSA is governed by a photosynthesis (P) versus photon flux density (E) curve with a fixed C:chl ratio for the PSA pool (χ_{chl}) (Geider et al., 2009). The maximum rate of photosynthesis (P^m_{PSA}) is normalized to PSA carbon (which is equivalent to normalizing to chlorophyll). The model has a constant chlorophyll specific initial slope (α^{chl}) of the P versus E curve that applies to both photosynthetic pathways (lpet and aet) and is expressed as

$$v_{\mathrm{aet}} + v_{\mathrm{lpet}} = \phi_{\mathrm{PSA}} P^m_{\mathrm{PSA}} \left(1 - e^{-E/E^*_k}\right) \text{ where } E^*_k = \frac{P^m_{\mathrm{PSA}}}{\alpha^{\mathrm{PSA}}} \tag{4}$$

where ϕ_{PSA} is the carbon content allocated to the PSA pool and P^m_{PSA} is the maximum photosynthetic rate in units of mol O_2 day per cell at a given temperature and α^{PSA} is the initial slope normalized to ϕ_{PSA} such that $\alpha^{\mathrm{PSA}} = \alpha^{\mathrm{chl}}/\chi_{\mathrm{chl}}$. The maximum achievable rate of photosynthesis thus depends linearly on allocation to PSA.

Calvin cycle carbon fixation (cal) is directly linked to lpet (i.e., cal = lpet). The RIB pool responsible for biosynthesis (syn) has a fixed efficiency (a_{syn}) such that the rate of syn (v_{syn}) is proportional to allocation to RIB (ϕ_{RIB}), with a fraction of fixed carbon consumed by autotrophic respiration of carbon (R_{tot}). For nondiazotrophs $R_{\mathrm{tot}} = R_0 = 0.5$. Growth rate ($\mu$) is equal to v_{syn} normalized to total cell carbon (C_m).

$$v_{\mathrm{syn}} = \phi_{\mathrm{RIB}} a_{\mathrm{syn}} (1 - R_{\mathrm{tot}}) \text{ and } \mu = \frac{v_{\mathrm{syn}}}{C_m} \tag{5}$$

2.4. Allometry

Several cell properties scale with cell size. Cell carbon content is prescribed as a power law function of cell volume based on compiled observations such that C scales as V^{γ}. The power law scaling, γ, has been estimated as 0.931, for nondiatom protists and 0.811 for diatoms (Menden-Deuer & Lessard, 2000). Metabolic rates also have been observed to scale allometrically (Kleiber, 1932) as described by metabolic theory of ecology (Brown et al., 2004) which predicts that at a given temperature, metabolic rate (B) scales as

$$B \propto M^{\beta} \tag{6}$$

where M is individual size and β is the scaling coefficient equal to 3/4. Furthermore for phytoplankton, cell volume is a more appropriate measure of size than mass, given that metabolic theory of ecology assumes a constant organism density, but cell carbon scales allometrically as described above (López-Urrutia et al., 2006). In PCAM we combine carbon to volume scaling with metabolic theory of ecology to scale carbon-normalized photosynthetic and biosynthetic rates such that

$$a_{\mathrm{syn}} = T_{\mathrm{func}} a^{\mathrm{ref}}_{\mathrm{syn}} \left(\frac{V}{V_{\mathrm{ref}}}\right)^{\beta-\gamma} \tag{7}$$

where $a^{\mathrm{ref}}_{\mathrm{syn}}$ is the rate of biosynthesis at reference cell volume (V_{ref}) and temperature. Photosynthetic rate, P^m_{PSA}, scales similarly as $(V/V_{\mathrm{ref}})^{-0.06}$. The above metabolic scaling arguments support observations that maximum normalized photosynthetic rate and growth rate decrease with increasing cell size.

For the smallest autotrophic phytoplankton cells with radii < 1 μm, this trend does not hold. The overhead burden of nonscalable parts, such as the chromosomes, membranes, and most importantly, the cell wall is a primary limit on the metabolic rate of small cells. To represent this limitation, we model structural cell allocation as consisting of a constant internal fraction of cell carbon, plus a cell wall fraction that scales as a constant thickness, d, assuming spherical volume. The fractional volume can be expressed as

$$\phi^w_{\mathrm{STR}} = C_m \frac{V_{\mathrm{wall}}}{V} = C_m \left(1 - \frac{(r-d)^3}{r^3}\right) = C_m \left(1 - \frac{3d}{r} - \frac{3d^2}{r^2} + \frac{d^3}{r^3}\right) \tag{8}$$

The cell wall component only is a significant burden for small cells, as ϕ^w_{STR} approaches 0 for $d \ll r$. At small cell sizes, when d becomes a significant fraction of r, a simple surface area to volume scaling for the cell wall is inaccurate and the quadratic term in (8) ($-3d^2/r^2$) becomes increasingly relevant. The combined result of equations (6)–(8) is that maximum growth rate in PCAM is a unimodal function of cell size (Figure 2). The rate at which growth rate of larger cell sizes decreases with increasing cell volume is dictated by the $\beta - \gamma$ scaling in equation (7), which is significantly more negative for nondiatoms than diatoms (Menden-Deuer & Lessard,

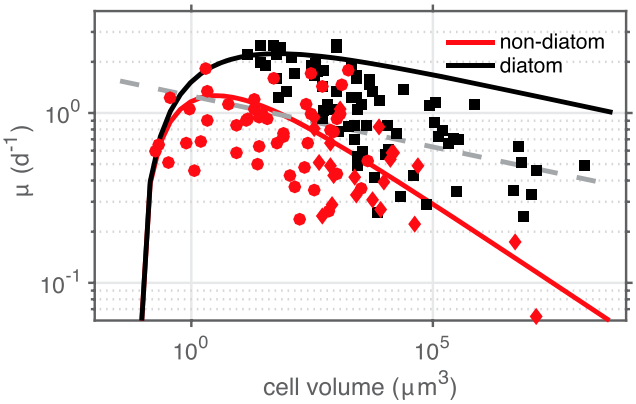

Figure 2. Phytoplankton growth rate as a function of cell volume. Data show a compilation of algal culture results digitized from Finkel et al. (2010). Diatoms are shown in black, dinoflagellates in red diamonds, and other taxa, including cyanobacteria, in red circles. The dashed gray line shows the least squares regression from Finkel et al. (2010). The solid black and red lines show PCAM solutions for diatoms and nondiatoms, respectively. For diatoms, PCAM uses a C:V power law scaling of 0.811 while nondiatoms using a power law scaling of 0.860, both from Menden-Deuer and Lessard (2000). PCAM conditions were $T = 25°C$, $E = 1000$, nitrate = 1 mM, phosphate 1 mM. PCAM = phytoplankton cell allocation model.

2000). Thus, the ability of diatoms to reduce carbon requirements affords them a competitive advantage that increases with size.

Observational evidence of allometric scaling of growth rate generally shows a slightly negative scaling exponent, despite significant scatter. Variability between taxa can be larger than allometric trends (i.e., diatoms generally having higher maximum growth rates than other taxa (Figure 2; Chisholm, 1992; Finkel et al., 2010). Some recent results support a unimodal function (Andersen et al., 2016; López-Sandoval et al., 2014; Marañón et al., 2013), which is consistent with the unimodal shape seen for PCAM in Figure 2.

2.5. Nutrient Uptake

Nutrient uptake in PCAM is based on a conceptual model of uptake sites (n), each with a fixed transporter site area (A) and a finite ion handling time (h) during which a site is unable to process additional nutrient ions (Aksnes & Egge, 1991; Fiksen et al., 2013; Lindemann et al., 2016) such that

$$V^S = \frac{n}{h}\frac{S}{(Akh)^{-1} + S} \tag{9}$$

where k is transfer velocity and equal to diffusivity divided by cell radius and S is ambient nutrient concentration.

Cells acclimate to ambient nutrient conditions by increasing n under nutrient stress up to an allometrically constrained maximum (n_{max}). Cell surface area to volume result in allometric scaling of nutrient affinity such that smaller cells outcompete larger cells at low nutrient levels as outlined in detail in the supporting information. Volume-normalized affinity scales as r^{-1}, while C-normalized affinity scales as $r^{-\gamma}$. Thus, the C:V scaling described in section 2.4 somewhat reduces the size dependency of nutrient uptake affinity.

The PCAM version presented here considers macronutrients in the form of nitrate and phosphate, as these are the most abundant available forms of inorganic N and P in the open ocean. Future development could include utilization of organic P and N substrates as well as the redox benefits of ammonium assimilation when present. Canonically, ammonium is preferred to nitrate, because nitrate requires reduction by an additional 8 electrons before it can be incorporated. Although this requires additional reductant to be generated via the lpet pathway, this cost is somewhat offset because the additional ATP generated by additional lpet activity reduces the level of aet activity needed for supplementary ATP supply. Based on PCAM stoichiometry, the net effect is a <6% decrease in necessary PSA allocation for growth supported by ammonium assimilation compared to growth on nitrate. This result is in agreement with culture studies that have attributed about 5% of gross photosynthesis to direct reduction of nitrate and sulfate (Fisher & Halsey, 2016). Previous studies have shown conflicting conclusions on the relative efficiency of phytoplankton growth on ammonium versus nitrate (Caperon & Ziemann, 1976; Dortch, 1990; Eppley et al., 1969; Thompson et al., 1989). Nitrate reduction does not appear to be a primary demand for phytoplankton metabolism, and we leave a full exploration of the trade-offs of nitrate versus ammonium for a future investigation.

2.6. Iron

Only a small fraction of iron in the ocean is bioavailable. Dissolved iron [Fe], operationally defined as the fraction passing through a 0.2 micron filter, includes both truly dissolved and colloidal components (Boyd & Ellwood, 2010). In PCAM, we model Fe uptake using the same framework as for macronutrients, assuming that the total dissolved fraction [Fe] is the form available for uptake. For trace elements such as Fe, significantly greater flexibility in uptake is possible (Morel, 1987), represented in PCAM by the larger range between K_{μ}^{Fe} and K^{Fe} (Figure S1).

Because of the high iron quota of the photosynthetic apparatus (PSA), a range of strategies has been observed for cells to restructure their PSA in response to iron stress. While cellular response to iron stress is multifaceted, we attempt a simplified representation that retains the core ability of a cell to reduce iron quota in PSA in response to iron stress with an associated trade-off in photosynthetic performance. In PCAM, iron

quota can be reduced by reducing overall allocation to PSA and is further reduced using a strategy that has been observed in iron-stressed phytoplankton in which photosynthetic reaction centers are disconnected reducing iron content in PSA in addition to lowering photosynthetic performance while retaining pigment and carbon (Behrenfeld & Milligan, 2013; Moseley, 2002). In PCAM, each photosynthetic pathway (lpet and aet) is assigned a distinct reaction stoichiometry (e^-:C:ATP; see equations (1) and (3)). PSA maximum iron quota ($Q^{Fe}_{PSA-max}$) is

$$Q^{Fe}_{PSA-max} = \phi_{PSA} r^{Fe:C}_{PSA} \tag{10}$$

Cells can further reduce iron quota by disconnecting photosynthetic reaction centers (Behrenfeld & Milligan, 2013; Riethman & Sherman, 1988) with the trade-off of lowering maximum photosynthetic rate:

$$Q^{Fe}_{PSA} = f_{con} Q^{Fe}_{PSA-max} \text{ and } P^{m}_{PSA} = f_{con} P^{ref}_{PSA} \tag{11}$$

where f_{con} is the fraction of reaction centers connected. PCAM could be refined in the future to further distinguish between aet pathways such as cyclic photosynthetic electron transfer, which is associated with PSI and has a high iron quota and high ATP yield and PSII pathways such as those directed to midstream oxidases that have lower iron demand but at the cost of lower ATP yield (Behrenfeld & Milligan, 2013). As iron availability decreases, PSII pathways will become more favorable relative to PSI pathways. Due to lack of observational constraints of this shift, we limit PSA in PCAM to have a single aet pathway and primarily alter its Fe quota via disconnecting photosynthetic reaction centers.

2.7. Diazotrophy

Diazotrophs in PCAM are implemented using a model core identical to that described above with the following additions: (1) An additional functional pool with high iron quota that includes nitrogenase, (2) an additional energetic demand for nitrogen fixation of 8 ATP per mole of nitrogen atoms fixed, and (3) an cost associated with reducing or removing dissolved oxygen to maintain hypoxic conditions within the cell, a requirement for nitrogenase functioning (Großkopf & LaRoche, 2012). The ATP demand due to a requirement of 16 ATP necessary to overcome the activation energy barrier to break a stable, N-N triple bond to produce two NH_3.

$$N_2 + 8H^+ + 8e^- + 16ATP \xrightarrow{yields} 2NH_3 + H_2 + 16ADP + 16P_i \tag{12}$$

Thus, low oxygen, high light, and high iron all are favorable for nitrogen fixation. ATP demand and Q^{Fe}_{NIT} are both proportional to the rate of nitrogen fixation (Kustka et al., 2003). The fraction of fixed carbon consumed by autotrophic respiration (R_{nfix}) associated with maintaining an anaerobic environment for nitrogen fixation scales linearly with the ambient dissolved oxygen saturation such that

$$R_{nfix} = \left([O_2]/[O_2]_{eq}\right) R^{max}_{nfix}. \tag{13}$$

Because nitrogenase is not a major fraction of cell mass (Whittaker et al., 2011), NIT is considered to have zero C, N, and P quotas. This simplification reduces model complexity and eliminates a free parameter. We do not distinguish here between diazotrophic strategies employing temporally separated nitrogen fixation (i.e., during nighttime) versus spatially separated (i.e., heterocysts), assuming that the strategies have approximately equal energetic balances over the 24-hr period. For unicellular cyanobacteria such as *Crocosphaera watsonii*, N_2 fixation occurs at night and the reducing equivalents needed to maintain a low oxygen environment thus must come from dark respiration of carbohydrates.

2.8. Optimal Allocation

Under balanced growth, inputs of photosynthate and nutrients to a cell are equal to use of these inputs by autotrophic respiration and net growth. For any given environmental condition, our model has a unique and optimal solution for the allocation of cell resources to PSA, RIB, (and NIT for diazotrophs). First, focusing on a single nutrient, *S*, we can write a system of model equations relating three unknowns. One equation relates the rate of linear photosynthetic carbon fixation (v_{lpet}) to the rate of biosynthesis (v_{syn}), taking into account autotrophic respiration and the constant fraction of base autotrophic respiration (R_0) during nitrogen fixation (R_{nfix}):

$$v_{syn} = v_{lpet}(1 - R_{tot}) \text{ where } R_{tot} = R_0 + R_{nfix} \tag{14}$$

A second equation balances ATP production via photosynthetic pathways with ATP demand from Calvin cycle and nitrogen fixation, noting that lpet and cal are linked at 1:1 ratio based on an $NADP^+$/NADPH redox balance (Geider et al., 2009):

$$v_{\mathrm{aet}}A_{\mathrm{aet}} + v_{\mathrm{lpet}}\left(A_{\mathrm{lpet}} + A_{\mathrm{cal}}\right) + v_{\mathrm{nfix}}A_{\mathrm{nfix}} = 0 \tag{15}$$

where v_{nfix} is the rate of nitrogen fixation (mol N/s per cell) and v_{aet} is the rate of the alternative electron transfer pathway aet (mol rxn/s per cell). Note that the sign of each ATP term is positive for ATP production (A_{aet} and A_{lpet}) and negative for consumption (A_{cal} and A_{nfix}). Units of A_x terms are mol ATP (mol rxn)$^{-1}$. Note that in PCAM there is no direct ATP demand associated with nutrient uptake, and ATP generation by autotrophic respiration is assumed to meet ATP demands of biosynthesis.

Growth rate is related to nutrient uptake such that

$$V^S = \mu^S Q^S_{\mathrm{tot}} = \frac{v_{\mathrm{syn}}}{C_m} Q^S_{\mathrm{tot}} \text{where } \phi_{\mathrm{tot}} = C_m = \phi_{\mathrm{PSA}} + \phi_{\mathrm{RIB}} + \phi_{\mathrm{STR}} + \phi_{\mathrm{STO}} \tag{16}$$

where cell quota relates to allocation (Table 2) such that

$$Q^S_{\mathrm{tot}} = \phi_{\mathrm{PSA}} r^S_{\mathrm{PSA}} + \phi_{\mathrm{RIB}} r^S_{\mathrm{RIB}} + \phi_{\mathrm{STR}} r^S_{\mathrm{STR}} + Q^S_{\mathrm{nfix}} \tag{17}$$

Nitrogenase quota (Q^S_{nfix}) is only active for diazotrophs and contributes only to cell iron quota, and nitrogenase is assumed a negligible contributor to cell whole-cell C, N, and P budgets. The rate of nitrogen fixation, v_{nfix}, is proportional to nitrogenase Fe quota, $Q^{\mathrm{Fe}}_{\mathrm{nfix}}$ such that $Q^{\mathrm{Fe}}_{\mathrm{nfix}} = r^{\mathrm{Fe}}_{\mathrm{nfix}} v_{\mathrm{nfix}}$ where $r^{\mathrm{Fe}}_{\mathrm{nfix}}$ has units of mol Fe (mol rxn)$^{-1}$.

The above set of equations can be solved for each potential limiting nutrient (N, P, and Fe) with optimal allocation equal to the solution with minimum (most limited) growth rate. Numerically, the solution for N and P limitation can be expressed as a quadratic equation with respect to ϕ_{RIB} and explicitly solved (see supporting information for derivation). For Fe limitation, the system of equations is nonlinear and solutions were determined using the MATLAB *fsolve.m* solver with the default "trust-region-dogleg" algorithm. This solver is iterative and thus has a significant and variable computational cost. On average, solutions without calculating Fe limitation require about one twentieth of the time.

3. Results

3.1. Light and Macronutrient Limitation

We compare the PCAM balanced growth solution against a range of laboratory and field data to evaluate how cell allocation (i.e., chl:C) and growth rate varies over a range light and macronutrient concentrations. Identical PCAM parameters (Table 1) are used in each of the below analyses.

3.1.1. Comparison With Laboratory Studies

Under low irradiance, such as during winter, periods of deep mixing, or in the deep stratified euphotic zone, solar energy to drive photosynthesis becomes a limiting resource. Phytoplankton are able to acclimate through levels of irradiance 2 to 3 orders of magnitude below optimal levels through acclimation strategies such as increasing the size and number of photosynthetic antennae complexes. Our model represents this acclimation by assigning a fixed chl:C ratio to the PSA component but allowing carbon allocation to PSA to vary. Thus, whole cell chl:C varies with shifting allocation as described in equations (14)–(17). While chlorophyll *a* normalized photosynthesis (lpet + aet)/chl is dictated by irradiance, plankton can maintain higher growth rates by increasing allocation to PSA. As irradiance decreases the optimal ratio $\phi_{\mathrm{PSA}}/\phi_{\mathrm{RIB}}$ needed to balance reductant and ATP increases. Acclimation to low irradiance allows the saturation irradiance for net growth (E^{μ}_k) to be significantly less than the chlorophyll normalized saturation irradiance for photosynthesis (E^*_k). While E^*_k is a fixed cell trait, E^{μ}_k is a function of cell acclimation state and can vary with time. Our model reproduces observed patterns in chl:C observed in continuous cultures of *Thalassiosira fluviatilis* and *Thalassiosira pseudonana* grown under decreasing irradiances (decrease in light-limited growth rate; Fisher & Halsey, 2016; Laws & Bannister, 1980; Figure 3). Because cell sizes were not specified and likely variable, we used a constant cell radius of 5 μm for comparison to diatom cultures. Results are not sensitive to varying this cell size due to the low cell size versus growth rate dependence (Figure 2).

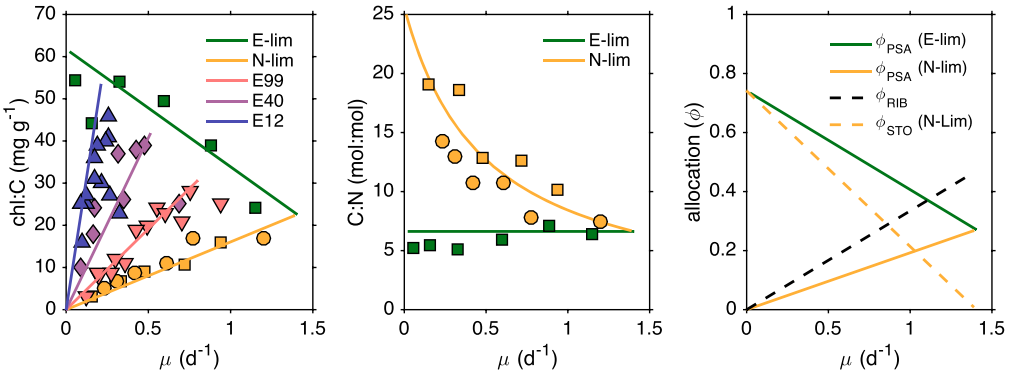

Figure 3. PCAM response for balanced growth limited by light (green) and nitrogen (gold) compared to equivalent laboratory data from continuous culture for the diatom *Thalassiosira fluviatilis* grown at 20 °C (squares; Laws & Bannister, 1980) for (a) chl:C acclimation. Light-nitrate-colimited growth is also shown for diatom *Skeletonema costatum*, grown in nitrate-limited continuous culture at 15 °C (Sakshaug et al., 1989). Light levels were 600 (gold circles), 99 (downward pointing pink triangles), 40 (purple diamonds), and 12 μmol photons · m^{-2} · s^{-1} (upward pointing blue triangles). (b) C:N stoichiometry. Squares are from Laws and Bannister (1980), and circles are from Sakshaug et al. (1989). (c) Functional pool allocation. Note that growth versus allocation to RIB is identical for light and nutrient limitation. In (a) lines indicate PCAM solutions under corresponding conditions. A cell radius of 5 μm was assumed for PCAM results.
PCAM = pshytoplankton cell allocation model.

The response of phytoplankton composition to growth under nitrogen limitation is strikingly different from that under light limitation. For example, in the culture studies by Laws and Bannister (1980) and Halsey et al. (2010, 2012), increasing levels of nitrogen limitation led to linear decrease in the chl:C ratio, the opposite trend as observed during light limitation (Figure 3a). Colimitation by light and nutrients leads to a similar linear response but with a steeper slope (Sakshaug et al., 1989). The trend associated with nutrient limitation is explained by the physiological response of reducing allocation to both PSA and RIB pools. When nutrients limit growth, there is no advantage for a cell to maintain large investments in light harvesting and biosynthetic capabilities (Figure 3c). Reducing the size of these pools reduces the overall cell nitrogen quota, allowing for a higher growth rate to be maintained for a given amount of nitrogen uptake relative to the growth rate that would be achievable by a cell retaining the PSA and RIB investments needed for replete growth. Acclimation (by reallocating cell resources) allows plankton to maintain a half saturation for growth rate (K^S_μ) at significantly lower ambient nutrient concentration than the half saturation for instantaneous uptake (K^S) (Morel, 1987). Another saturation term, $K^S_{\mu Q}$ is defined as the nutrient concentration at which the product of μ and Q^S is half its maximum (Morel, 1987). Figure S1 illustrates the relationship between these saturation thresholds in PCAM.

3.1.2. Comparison to Field Data

Net primary productivity in carbon units (N_C) is a critical variable in the study of ocean ecosystems, biogeochemistry, and the carbon cycle. In PCAM, N_C per cell is equal to v_{syn}. Table 3, and N_C normalized to carbon biomass, is equivalent to growth rate, μ. Radiocarbon-labeled primary productivity incubations (Steemann Nielsen, 1952; PP(^{14}C)) are the most widespread field measurement of ocean primary productivity, and when

Table 3
Equations for the Rate of Each Metabolic Pathway (mol rxn per cell/day)

Symbol	Description	Value
v_{aet}	Alternative photosynthetic pathway	$v_{aet} = P^m_{PSA}\left(1 - e^{E\chi_{chl}/\left(P^m_{PSA}\alpha_{chl}\right)}\right)\phi_{aet}$
v_{lpet}	Linear electron photosyn. transport	$v_{lpet} = P^m_{PSA}\left(1 - e^{E\chi_{chl}/\left(P^m_{PSA}\alpha_{chl}\right)}\right)\phi_{lpet}$
v_{cal}	Calvin cycle C fixation	$v_{cal} = v_{lpet}$
v_{syn}	Biosynthesis	$v_{syn} = a^m_{syn}\phi_{RIB}$

conducted over longer periods (i.e., 6–24 hr) best corresponds to N_C (Marra, 2009). Predicting N_C using algorithms based on satellite observations and from ocean biogeochemistry models has been proven to be challenging (Friedrichs et al., 2009; Saba et al., 2010). Because the PCAM can be solved explicitly for the case of balanced growth limited by light and/or macronutrients, we are able to evaluate model skill in predicting field observations of net primary productivity (N_C) when the necessary input variables (PAR, chlorophyll, nutrients, and temperature) are provided.

We test the ability of PCAM (configured for nondiazotrophs) to predict N_C based on the relationship,

$$N_C = \frac{\mu^{\mathrm{PCAM}}(\mathrm{chl})^{\mathrm{OBS}}}{(\mathrm{chl}:C)^{\mathrm{PCAM}}} \tag{18}$$

where $(\mathrm{chl})^{\mathrm{OBS}}$ is a field measurement of chlorophyll and μ^{PCAM} and $(\mathrm{chl{:}C})^{\mathrm{PCAM}}$ are PCAM-predicted growth rate and chlorophyll to carbon ratios, respectively. PCAM μ and (chl:C) are calculated from observed temperature, nitrate, phosphate, and photosynthetically available radiation (PAR) at discrete measurement depths through the upper ocean as outlined in the model description using the same parameter values as used in section 3.1.1 (Table 1). Values of N_C are also computed using SatPPMs, which rely on surface remote sensing products (e.g., chlorophyll, irradiance, and temperature) and extrapolate to depth. Because phytoplankton size spectra were not available for these observations, we assumed a constant cell radius of 3 μm. As remote-sensed phytoplankton size distribution algorithms mature, we expect that they could be incorporated into analyses such as this (Kostadinov, 2016; Mouw et al., 2017).

We compare PCAM results with field observations from the JGOFS and CalCOFI programs. The JGOFS analysis covers the greatest range of biogeochemical conditions and is detailed here, while the analysis using CalCOFI data, which include depth, resolved observations including measured PAR attenuation, is detailed in the supporting information. Six U.S. JGOFS process cruises from 1989 to1998 measured PP(^{14}C) and the necessary variables to evaluate the PCAM over a wide range of oceanic regimes. The JGOFS Process Studies (Doney et al., 2001; Knap et al., 1996) included sites in the Equatorial Pacific, Arabian Sea, Southern Ocean, and North Atlantic and were designed to improve understanding of biogeochemical processes by including a suite of standardized measurements, which included 24-hr ^{14}C PP, chlorophyll, nitrate, phosphate, temperature, and mixed layer depth. Mixed-layer mean values for the process cruises have been compiled as part of a synthesis and modeling project (Doney et al., 2001; Kleypas & Doney, 2001), and we use data from all stations where all of the above-mentioned variables were measured. PAR was not reported for the JGOFS sites, however. For the PCAM and SatPPM calculations we instead used 9-km monthly climatological PAR from Moderate Resolution Imaging Spectroradiometer MODIS-Aqua. Surface PAR was selected from the nearest grid point for each observation and linearly interpolated to the day of year of the observation. Mean-mixed layer PAR was calculated using mixed-layer chlorophyll values and a PAR attenuation model (Morel & Maritorena, 2001).

Additionally, PCAM was compared to two SatPPMs, the Vertically Generalized Productivity model (VGPM) that depends on chlorophyll, temperature, and PAR (Behrenfeld & Falkowski, 1997) and the Eppley model (EPPLEY) that is a function of chlorophyll alone (Eppley et al., 1985). VGPM is the most widely used algorithm, while EPPLEY is the simplest yet has been demonstrated to have skill comparable to many more complex models (Friedrichs et al., 2009). The EPPLEY model has a single free parameter, while the VGPM includes 23 parameters. For VGPM and EPPLEY evaluations, in situ chlorophyll was used rather than remote-sensed chlorophyll.

Although the PCAM has more degrees of freedom, it does a better job of reproducing JGOFS observations compared to VGPM and EPPLEY models. The PCAM output exhibits positive correlation with observations for all JGOFS sites (Figure 4). Systematic biases between sites also appear to be reduced. Predicted N_C at oligotrophic Hawaii Ocean Time-series (HOT) and Bermuda Atlantic Time-series Study (BATS) is reduced for PCAM but with improved correlation compared to VGPM, likely due to the inclusion of nutrient data in PCAM. A tendency toward model underestimation in low-latitude upwelling regions (EQPAC and ARABIAN) appears present in all models. Recent analyses suggest that the commonly used Eppley (Eppley, 1972) temperature dependence of phytoplankton growth (T_{func} in PCAM) is too strong, which may explain this discrepancy (Sherman et al., 2016). Model skill is evaluated using several metrics including root-mean-square difference (RMSD), centered pattern RMSD ($\mathrm{RMSD_{CP}}$) and bias (B) (Friedrichs et al., 2009). $\mathrm{RMSD_{CP}}$ is equivalent to RMSD once the bias has been removed. Following previous primary production model evaluations

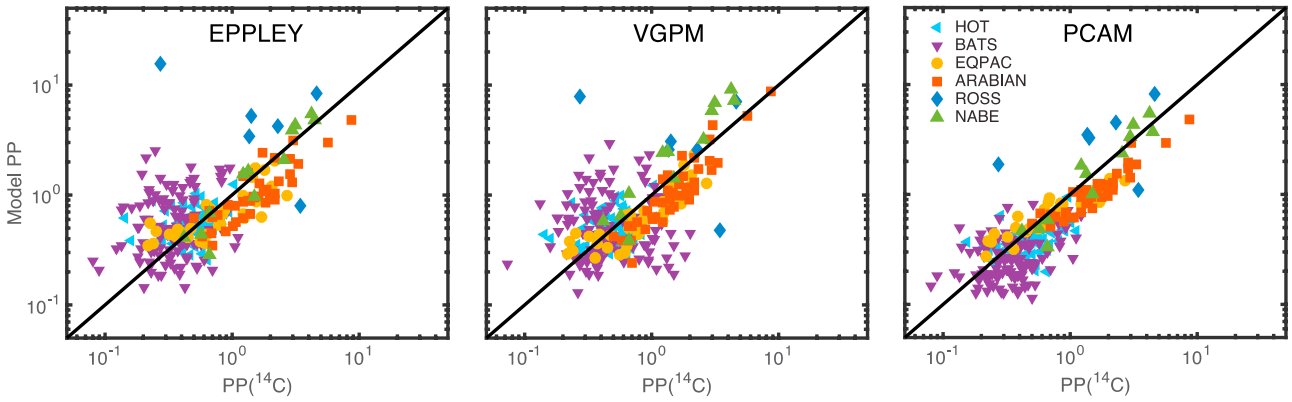

Figure 4. PCAM primary productivity (mmol C · m^{-3} · d^{-1}) compared to the vertical generalized productivity model (VGPM) and the EPPLEY squared model (EPPLEY) for six JGOFS sites. PCAM PP is the product of PCAM specific growth rate, C:chl (assuming balanced growth) and observed chlorophyll ($PP = chl_{obs}\mu_{PCAM}(C/chl)_{PCAM}$). Each algorithm is evaluated against observed field measured primary productivity based on 12- or 24-hr ^{14}C incubations. Iron was not measured and is assumed replete. PCAM = pshytoplankton cell allocation model; JGOFS = Joint Global Ocean Field Study.

(Friedrichs et al., 2009; Saba et al., 2011), model-data misfit is calculated on $\log_{10}$ transformed primary production. A Taylor Diagram (Figure 5) summarizes statistics of correlation, *R*, standard deviation and $RMSD_{CP}$, illustrating that PCAM has a superior fit when compared to VGPM and EPPLEY at most sites and for the pooled JGOFS data set.

3.2. Diazotrophy and Iron Limitation

3.2.1. Comparison With Laboratory Studies

C. watsonii is a single-cell, free living diazotrophic cyanobacteria approximately the same size as the nondiazotrophic cycanobacteria *Synechococcus*. Comparing model analogues of these two otherwise similar microbes provides insights into the trade-offs associated with nitrogen fixation. Two model organisms, CW and SYN, were initialized with the same 1-μm radius and model parameters, differing only in the presence/absence of nitrogen fixation. Other than cell size, we applied the same model parameters used in section 3.1 except for an ATP demand for dinitrogen fixation (A_{nfix}), an iron quota for nitrogenase (Q^{Fe}_{NFIX}), and respiratory demand to remove oxygen (R_{nfix}). First, we compare the diazotrophic model organism (CW) to

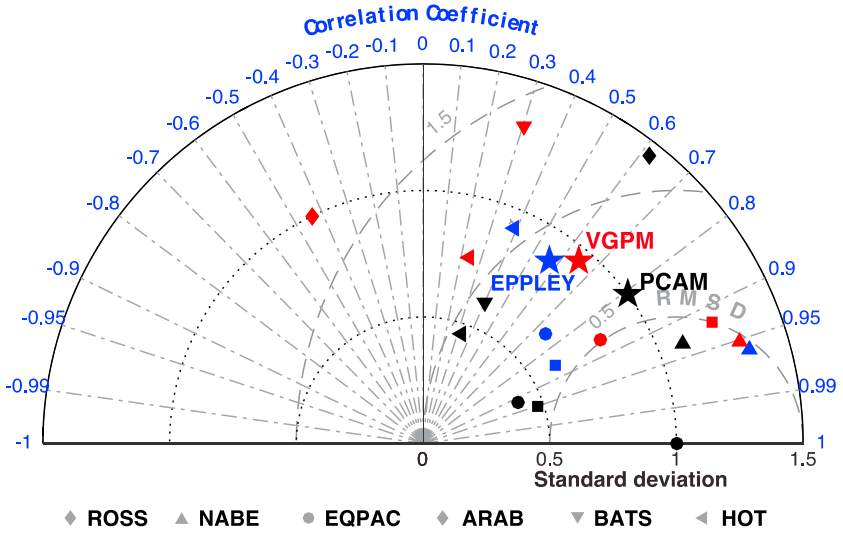

Figure 5. Taylor diagram showing skill of VGPM, EPPLEY, and PCAM in estimating observed volumetric ^{14}C primary productivity from JGOFS. For all locations pooled (large stars), PCAM had the lowest $RMSD_{CP}$ error and highest correlation coefficient. VGPM = vertical generalized productivity model; PCAM = pshytoplankton cell allocation model; JGOFS = Joint Global Ocean Field Study; RMSD =root-mean-square difference.

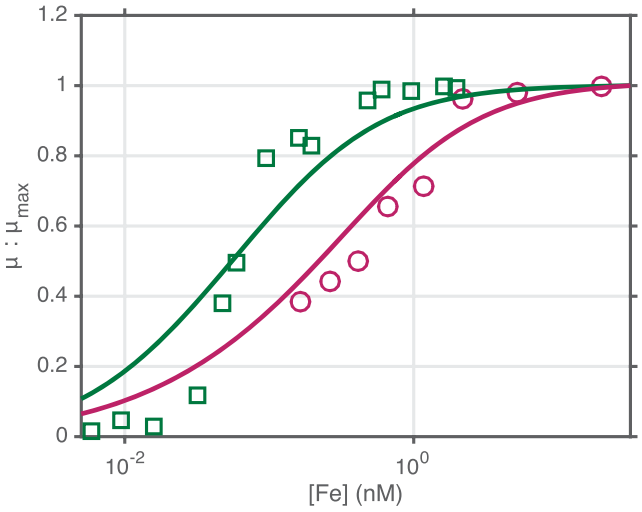

Figure 6. Normalized iron-limited growth in continuous culture for the diazotroph *Crocospherae watsonii* (magenta; Jacq et al., 2014) and for the coastal *Synechococcus bacillaris* (green; Sunda & Huntsman, 1997, 2015). Solid lines show pshytoplankton cell allocation model-balanced growth solutions for a diazotroph (magenta) and nondiazotroph (green). Although nutrient uptake kinetics are identical, the diazotroph has additional Fe requirements. Cell radius of 1 μm is assumed for both *Synechococus* and *Crocospherae* watsonii model analogues.

iron limited growth of *C. watsonii* under culture conditions (Jacq et al., 2014). PCAM reproduces iron-limited growth as observed in batch culture over a range dissolved iron concentrations (Figure 6). Diazotrophy requires higher iron quota both for nitrogenase directly and for greater allocation to PSA for alternative electron transport pathways that support higher ATP demand. Nitrogenase iron quota is directly proportional to N-fixation rate. The greater iron quota is reflected in the relative competitive advantage of SYN over CW under Fe stress (Figure 6), an observation supported by iron-limited chemostat studies of *Synechococcus* (Sunda & Huntsman, 1997).

3.2.2. Comparison With Field Observations

The GEOTRACES intermediate data product (IDP2014v2) (Mawji et al., 2015) includes the full suite of environmental variables, including dissolved Fe, needed to solve PCAM, assuming balanced growth. Here we evaluate PCAM for two basin-scale transects in the Atlantic. The first, GA03, was completed in 2010 and 2011 on the *R/V Knorr* between Woods Hole, MA, and the Mauritanian upwelling zone (Boyle et al., 2015). The second, GA02, was a meridional section stretching along the western side of the Atlantic Basin from the Irminger Sea to Puntas Arenas, Chile, completed in three legs during 2010 and 2011 aboard the *R/V Pelagica* and *RRS James Cook* (Rijkenberg et al., 2014). As surface PAR was not recorded for these sections, we combined MODIS-Aqua 9 km daily PAR with measurements of water column attenuation. Water column attenuation was calculated from integrating CTD transmissometer data at each station as part of IDP2014v2 release. PCAM-balanced growth (Figure 7) was calculated for each sampling location and depth where all necessary variables were available (Figure S3). For the zonal GA03 section, Fe was generally too low for diazotrophs to thrive in the surface layer, yet a niche favorable for diazotrophs was present directly below at 30–40 m. For GA02, Fe availability (Figure S3) strongly dictates the growth rate of both with CW and SYN, with presumably dust-born input north of the equator, similar to what has been observed in Atlantic Meridional Transect program observations (Moore et al., 2009). Additionally, a potential shelf source of iron is evident near 30°S where CW is favored near the surface, consistent with new evidence of nitrogen fixation in this region (Moore et al., 2014).

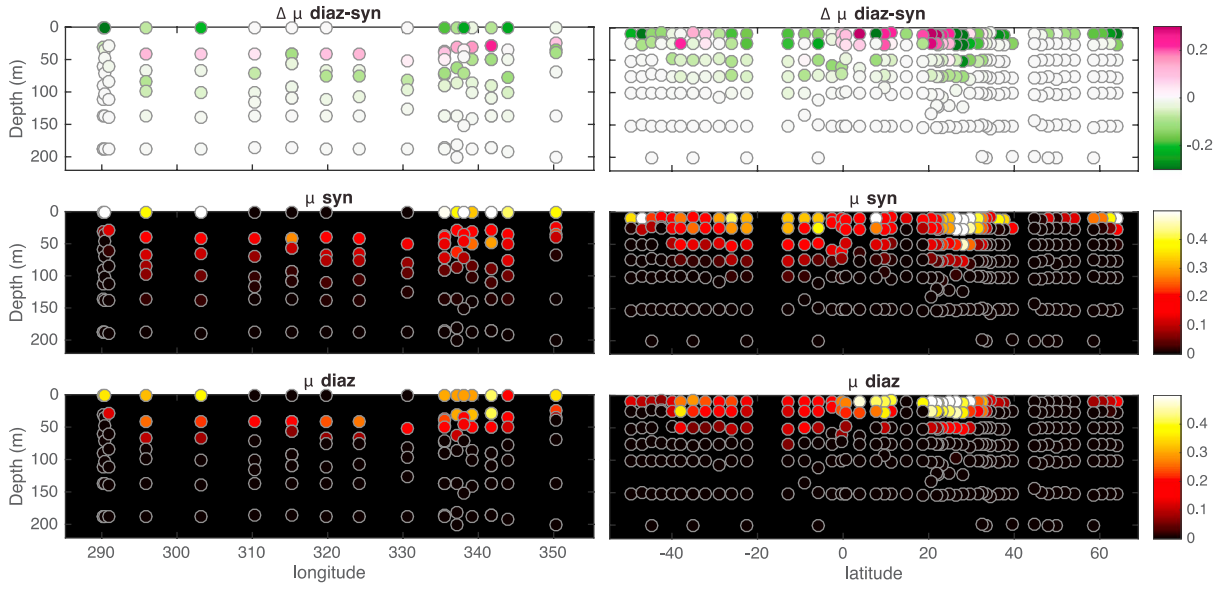

Figure 7. Growth rate for balanced growth pshytoplankton cell allocation model solution for model *Crocospherae watsonii* and *Synechococcus* analogues compared for GEOTRACES ga03 (left) and ga02 (right) sections with the difference in growth rate shown in the top panels.

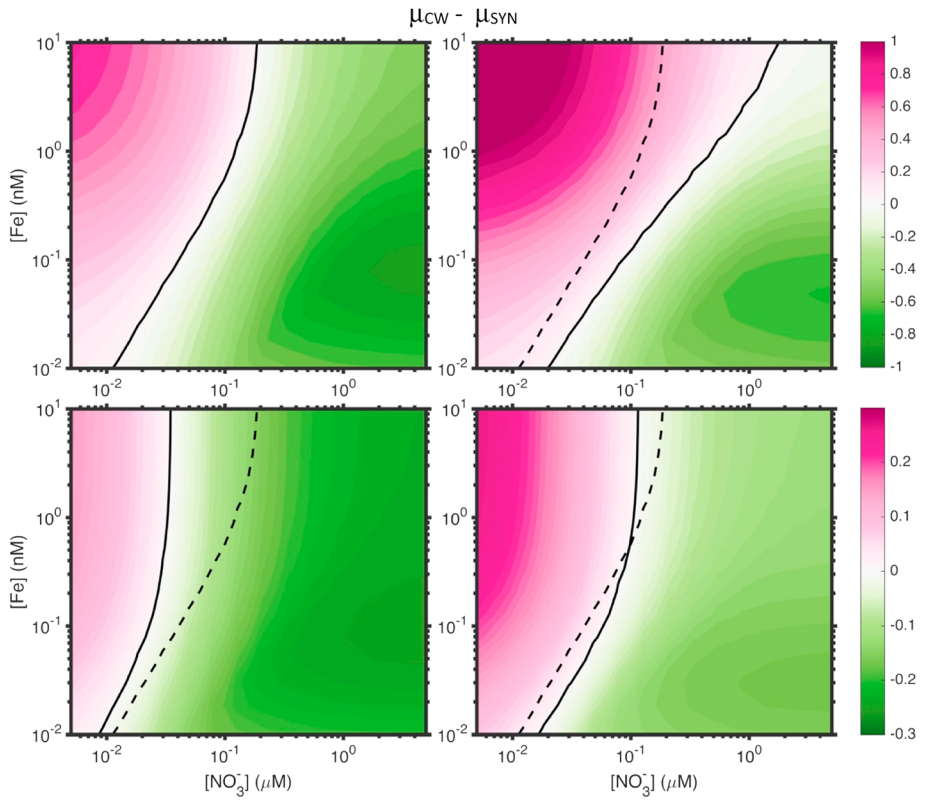

Figure 8. Nondiazotrophic minus diazotrophic growth (Δμ) as a function of nitrate and iron are shown for (a) replete light (1,000 μmol quanta · m^{-2} · s^{-1}; b) replete light plus low O_2 (O_2sat = 10%; c) low light (40 μmol quanta · m^{-2} · s^{-1}), and (d) under both low light and low O_2. Magenta shaded parameter space favors diazotrophs (CW) and green shades show where nondiazotrophs are favored (SYN). Black solid lines show the zero contour for each panel. The zero contour for replete conditions from panel (a) is shown as a dashed line for reference in other panels.

3.2.3. Diazotrophy Niche

The above results illustrate the high iron, low nitrate + ammonia niche that is favorable for diazotrophs (Figure 8). The size of this Fe-N niche space can be modulated by other resources/stressors. For example, under saturated oxygen conditions (pO_2 ~ 0.2 atm), the requirement to maintain an anoxic site for nitrogen fixation is a major metabolic cost for diazotrophs, directly accounting for approximately 60% of cellular respiration when oxygen is at 100% saturation (Großkopf & LaRoche, 2012). Under low O_2 conditions, diazotrophs are released from this additional respiratory demand, significantly expanding their competitive niche into higher nitrate and lower Fe parameter space (Figure 8). The primary effect is a contraction of the diazotroph niche at high [O_2] (Figure 8). Compared to nonfixers, diazotrophs have a higher demand both for the energetic (ATP) cost of N_2 fixation and for the additional carbon fixation needed to support respiratory removal of O_2. Both demands contribute to higher allocation to PSA and thus a greater sensitivity to light limitation. Also, due to the combined impact of overall lower growth rate and high PSA allocation at low light, Fe quota is dominated by PSA. Even as photocenters are disconnected (see section 2.6) the low efficiency of active photocenters means that PSA continues to contain the majority of cell Fe quota. Under low light, NIT becomes a minor additional Fe requirement for diazotrophs relative to investment in PSA. The "Fe advantage" of nondiazotrophs is thus minimized when light is low.

4. Discussion

The PCAM represents cellular acclimation to environmental conditions through allocation of cell resources to a number of core functional pools. Using this core approach, we demonstrate the ability to model a range of laboratory and field observations of phytoplankton growth and composition. PCAM includes mechanistic details, such as variable stoichiometry and multiple photosynthetic pathways. The pathways represented

in PCAM can inform on the trade-offs associated with multiple limiting resources and stressors. PCAM provides a range of predictions, testable against measures of subcellular metabolism and composition.

4.1. On Net Versus Gross Photosynthesis

The gross to net photosynthetic ratio (N_C:G_{O2}) is an indicator of metabolic cell demands for photosynthate. Even under ideal conditions, a large fraction of gross photosynthesis (~60%) is allocated to processes including catabolism and alternative electron transport pathways. In PCAM, under replete conditions a cell has a base efficiency of 40% of gross photosynthesis ultimately allocated to growth (i.e., N_C:G_{O2} = 40%). This allocation efficiency appears to be representative of bulk phytoplankton communities in the field (Marra, 2002) as well as for a range of taxa in culture (Halsey & Jones, 2015). However, a wide variability certainly exists, a clear example of which is the low N_C:G_{O2} of diazotrophs as discussed more below. PCAM explores diazotrophy but does not yet include other potential trade-offs, such as motility and photoprotection (Fisher & Halsey, 2016; Halsey et al., 2014). With more observational constraints, PCAM could be enhanced in the future to add additional mechanisms for flexibility in N_C:G_{O2}.

Diazotrophy decreases N_C:G_{O2} due to the higher rate of autotrophic respiration. Thus, depending on functional type and iron availability varies from 12% to 40%. Results from productivity tracer studies hint at such physiologic flexibility (Juranek & Quay, 2013). A low N_C:G_{O2} could be either due to low N_C:G_C or low G_C:G_{O2}, depending on if O_2 reduction is accomplished directly through light-dependent processes such as the Mehler reaction or if carbon is fixed during daytime followed by subsequent dark respiration. Both cases have been observed in culture studies. Low G_C:G_{O2} ratios where observed in *Trichodesmium*, such that up to 70% of G_{O2} was attributed to Mehler Cycle activity to reduce O_2 (Kana, 1993; Milligan et al., 2007). In *C. watsonii*, a large diel variability in the carbohydrate pool has been observed, indicating substantial excess daytime photosynthesis and dark respiration is responsible for a low N_C:G_C (Dron, Rabouille, Claquin, Chang, et al., 2012; Dron, Rabouille, Claquin, Le Roy, et al., 2012). Either approach result yields a similarly low N_C:G_{O2} as predicted by PCAM for diazotrophy, but uncertainty remains in the relative contribution of autotrophic respiration versus aet for meeting oxygen removal demands. The choice of strategy to meet this demand may depend on the strategy for nitrogen fixation, as *C. watsonii* fixes nitrogen at night while *Trichodesmium* spatially segregates photosynthesis and nitrogen fixation, and actively fixes during the day.

For models to have a more realistic and mechanistic response to environmental conditions a measure of gross photosynthesis, particularly resolving alternative pathways, is critical yet seldom included in current models, which often bypass gross production altogether, favoring N_C as a starting point. The convention of modeling net primary production (N_C) in the marine environment, whether from using SatPPMs or in ESMs, is largely a historical result of ^{14}C incubations serving as the primary available validation data set by which models are evaluated. Given that the 12-24 hr ^{14}C incubation method is, ostensibly, most closely related to N_C (Marra, 2002, 2009; Quay et al., 2010), models sought to model a quantity that could be readily validated. Model equations underlying most SatPPMs and ESMs are derived from descriptions of photosynthesis more mechanistically linked to G_{O2} or G_C. Indeed, for terrestrial systems where tower measurements of G_C are the dominant source of validation (Baldocchi et al., 2001; Beer et al., 2010), modeling communities have focused on gross photosynthesis (Anav et al., 2013). Implicitly, ocean models neglect the dynamic relationship between gross and net photosynthesis which is central to many adaptive strategies employed by phytoplankton. PCAM represents a first and significant step toward addressing this shortcoming.

4.2. Trade-Offs of Diazotrophy

Diazotrophs are observed through much of the low-latitude ocean (Luo et al., 2014), usually as a minor constituent of the phytoplankton population, although in some cases, blooms dominated by *Trichodesmium* and other diazotrophs are observed (Capone et al., 1997; Sohm et al., 2011). Integrated into a full ESM, PCAM would provide a more mechanistic basis for predicting the growth, persistence and biogeography of diazotrophs in the context of complex ocean physics, trophic interactions, resource availability, and multiple stressors. Indeed, this is a goal for future PCAM development. Short of a full prognostic model, PCAM can still be interpreted diagnostically to yield interesting insights.

Resource competition theory predicts that for systems in steady state, diazotrophs can coexist with non-diazotrophs but can never dominate the population (Dutkiewicz et al., 2012; Tilman, 1982).

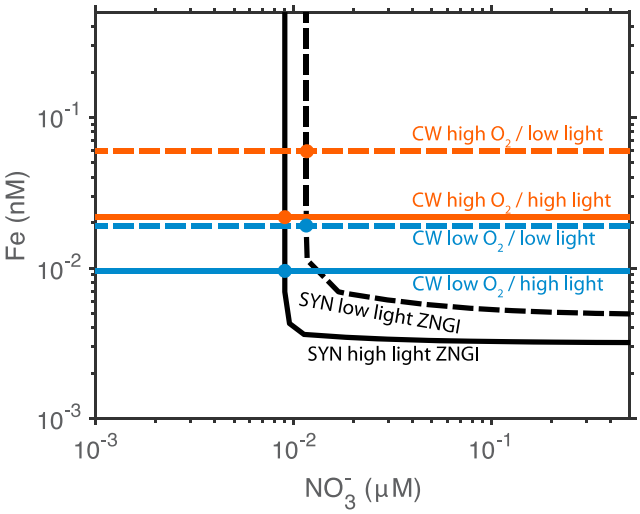

Figure 9. Zero net growth isolines are shown for model diazotroph (CW; orange and blue) and nondiazotroph (SYN; black). High light solutions are shown in solid lines and low light solutions are dashed. For CW, blue lines show 10% O_2sat solutions and orange lines show 100% O_2sat solutions. The dots indicate points where SYN and CW can coexist for steady state conditions based on resource competition theory.

Phytoplankton blooms, however, are transient and (assuming similar loss rates) will be dominated by the phytoplankton functional type with the highest growth rate. For diazotrophs, such a bloom could be triggered by, for example, an aeolian iron deposition event (Rubin et al., 2011). In the following discussion, we first apply PCAM to examine relative growth rates to assess conditions where diazotroph blooms could occur and then apply PCAM in a resource competition framework to assess conditions where stable persistence could occur. Each of these two frameworks have their own significant limitations for explaining the growth and persistence of phytoplankton and do not consider important factors including variability in top-down control, physical circulation and mixing, episodic nutrient injection, and other important processes present in a fully coupled model. Despite these limitations, preliminary insights can be gained both from assessing instantaneous growth rate and from applying resource competition theory.

4.2.1. Relative Growth Rate From Geotraces Sections

For a diazotroph, three primary costs associated with the ability to fix nitrogen are (1) the added ATP needed to split N_2, (2) the necessity to remove O_2 for nitrogenase activity, and (3) a higher iron quota associated with nitrogenase as well as additional photosynthetic activity required to meet challenges (1) and (2). In addition to fixed nitrogen availability, we identify light, oxygen, and iron as environmental variables that strongly influence the trade-offs of diazotrophy. In PCAM, each factor has a significant influence of the allocation of photosynthate and the N_C:G_{O2} growth ratio. The direct effect of the additional ATP demand is the necessity for higher allocation to aet pathways, with an associated iron quota. For diazotrophs, high oxygen, as is generally found in the surface euphotic zone, must be reduced or removed to maintain low oxygen around nitrogenase, leading to an additional respiratory demand that scales with ambient oxygen. The additional iron quota associated with nitrogenase disadvantages diazotrophs when iron is scarce. Using PCAM, the interactions between these multiple factors are combined to determine a competitive niche in parameter space in which diazotrophs are predicted to thrive. The analysis of Geotraces data (Figure 7) shows how the relative niches for CW and SYN in parameter space (Figure 8) can be mapped onto field observations to predict where conditions are favorable for diazotrophy (Figure 7).

4.2.2. Resource Competition Theory

The above analysis considers the relative fitness of *C. watsonii* versus *Synechococcus sp*. analogues for a "snapshot" of conditions but does not address if these conditions represent a stable environment or if observed conditions represent a transient condition. Resource competition theory (Tilman, 1982) provides a framework for predicting the phytoplankton class that will outcompete others under steady state conditions. For a given resource, a phytoplankton class will be excluded from the equilibrium solution if a resource falls below the minimum concentration (R^*) needed to support that class, as defined by the zero net growth isocline (ZNGI). The ZNGI is the resource isoline at which growth rate is just sufficient to match loss terms (i.e., grazing, assumed here a constant rate of 0.1/day). Dutkiewicz et al. (2012) applied resource competition theory to outline a framework for competition between diazotrophs and nondiazotrophs for nitrogen and iron. When considering competition for N and Fe, coexistence was shown to only be possible in one parameter-space location, where ZNGI lines for diazotrophs and nondiazotrophs intersect (Figure 9). Here we take the framework of Dutkiewicz and apply the PCAM to illustrate how light and oxygen could modify the ZNGI lines for each functional type and shift the location of the coexistence intersection. Previous applications of resource competition theory assume that R^* for a given resource is independent of other nutrients (implying there is no interdependency between Fe and N metabolisms, e.g.), resulting in no curvature in ZNGI lines. The PCAM solution shows curvature in the ZNGI connecting Fe limitation to N limitation indicating a region of colimitation, which is not represented in a theoretical model built upon Leibig's law of the Minimum. This curvature is due to the interactions and trade-offs in Fe versus N metabolism inherent in PCAM. The point in coexistence point in Fe-N space is located at slightly higher Fe and N concentrations when light is low. Oxygen, in

contrast, has a large impact on the lowest [Fe] viable for coexistence, with low O_2 enabling diazotrophs to persist at a significantly lower Fe*.

4.3. Future Applications

An ultimate application of PCAM would be the inclusion of such a model in a prognostic coupled ESM used to simulate past and future climate. Such integration faces a number of challenges. One is the added computational complexity. Several additional prognostic variables would be needed to track the internal allocation for each phytoplankton functional type. Furthermore, the optimal allocation solution described in section 2.8 requires an iterative solution when iron is considered. Such iteration would be computationally more challenging in an ESM. A possible strategy to overcome this limitation would be to use off-line computed lookup tables intelligently gridded in parameter space to bypass the iterative step. Such lookup approaches are applied in other ESM domains such as in atmospheric models to avoid computationally expensive online steps, for example, (Morrison et al., 2005). Another challenge is how to treat the physical mixing of members of a PFT that are differentially acclimated. An agent-based model approach (Grimm et al., 2005; Hellweger et al., 2014) in the Lagrangian frame would thus be a good match for a PCAM implementation.

Extending the use of PCAM as a diagnostic model is also a promising direction such as using it as a next-generation SatPPM. In addition to established photosynthetic parameters, a version of PCAM adapted as a SatPPM could take advantage of remote-sensed sun-induced fluorescence. Physiological responses to iron stress, including an increased PSII:PSI ratio and disconnected pigment complexes, increase fluorescent quantum yield, which in turn alters remotely observable sun-induced fluorescence (Behrenfeld et al., 2009). Beyond predicting NPP, PCAM would predict a number of additional parameters including chl:C and cell stoichiometry. As phytoplankton size satellite algorithms mature (Mouw et al., 2017), they could be used as inputs to drive the allometric underpinnings of PCAM.

Available validation data sets for PCAM and for models in general primarily consist of bulk measurements, such as primary productivity and whole-cell stoichiometry and chlorophyll content. A primary goal of PCAM is to serve as a hypothesis as to the mechanistic response of phytoplankton to the combined effect of multiple resources and stressors. Because functional pools and core metabolic processes are represented in PCAM, new classes of observational data could be applied as constraints on model performance (Doney et al., 2004) including a host of "omics" that illuminate the mechanisms of phytoplankton response to their environment and techniques that can quantify elemental allocation on the subcellular level, such as X-ray fluorescence-based techniques (Twining & Baines, 2013).

5. Conclusions

The PCAM presented here applies an optimal allocation framework to explain disparate observations of phytoplankton growth over a range of environmental conditions for diazotrophic and nondiazotrophic growth, which are demonstrated to require significantly different strategies for the allocation of photosynthate. Gross photosynthetic activity includes linear pathways directly linked to carbon fixation as well as ATP-generating alternative pathways. For nondiazotrophic growth, approximately 20% of G_{O2} is allocated toward aet pathways to supplement ATP requirements. An additionally, half of total fixed carbon (G_C) is subsequently consumed by mitochondrial respiration and catabolism, resulting in an overall photosynthetic use efficiency (N_C:G_{O2}) of about 40%. For diazotrophs, a much larger portion is devoted to alternative pathways due to the demand for energy for splitting dinitrogen and need to remove/reduce oxygen. Diazotroph N_C:G_{O2} is thus much lower, at around 12%.

Incorporating these trade-offs into a cell allocation model further informs on how photosynthate allocation impacts growth rate, including the effects of light, nitrogen, and iron limitation. Under replete conditions diazotrophs have a lower maximum growth rate. Furthermore, we argue that oxygen removal is the largest cause of the observed lower growth rate with the cost of splitting dinitrogen a secondary cause. These costs result in an optimal allocation solution for replete. Diazotrophic growth rate is about half of that of a nondiazotrophic analogue and requires about twice the allocation to PSA to achieve a given growth rate. A higher Fe quota due to both the larger PSA requirement and Fe needed for nitrogenase results in nondiazotrophic growth being more competitive under low Fe conditions. The competitive advantage is even greater at low light where PSA requirement is enhanced. Modeling such trade-offs over a wide range of

environmental conditions and resource limitations using minimal additional parameters requires a mechanistic approach. Here using a cell allocation model, we have demonstrated that the primary trade-offs of diazotrophy can be encapsulated using only three parameters that differ from how nondiazotrophs are represented; an iron quota for nitrogenase; a respiratory cost proportional to oxygen saturation; and an energetic cost for nitrogen fixation.

Acknowledgments
The authors gratefully acknowledge support from NOAA Global Carbon Program (NA100AR4310093) and Center for Microbial Oceanography Research and Education (CMORE; NSF EF-0424599). JGOFS data sets are archived by the Biological and Chemical Oceanography Data Management Office (BCO-DMO) and available at ftp://globec.whoi.edu/pub/software/JFOGS_GLOBEC. CalCOFI data that are used for this study can be found at http://calcofi.org/data.html. Geotraces data are available from geotraces.org, and for the IDPv2 2014 product used here can be found at www.bodc.ac.uk/geotraces/data/idp2014.

References

Aksnes, D. L., & Egge, J. K. (1991). A theoretical model for nutrient uptake in phytoplankton. *Marine Ecology Progress Series. Oldendorf*, *70*(1), 65–72.

Allen, J. F. (2003). Cyclic, pseudocyclic and noncyclic photophosphorylation: New links in the chain. *Trends in Plant Science*, *8*(1), 15–19. https://doi.org/10.1016/S1360-1385(02)00006-7

Anav, A., Friedlingstein, P., Kidston, M., Bopp, L., Ciais, P., Cox, P., et al. (2013). Evaluating the land and ocean components of the global carbon cycle in the CMIP5 Earth System Models. *Journal of Climate*, *26*(18), 6801–6843. https://doi.org/10.1175/JCLI-D-12-00417.1

Andersen, K. H., Berge, T., Gonçalves, R. J., Hartvig, M., Heuschele, J., Hylander, S., et al. (2016). Characteristic sizes of life in the oceans, from bacteria to whales. *Annual Review of Marine Science*, *8*(1), 217–241. https://doi.org/10.1146/annurev-marine-122414-034144

Anning, T., MacIntyre, H. L., Pratt, S. M., Sammes, P. J., Gibb, S., & Geider, R. J. (2000). Photoacclimation in the marine diatom *Skeletonema costatum*. *Limnology and Oceanography*, *45*(8), 1807–1817. https://doi.org/10.4319/lo.2000.45.8.1807

Armstrong, R. A. (1999). An optimization-based model of iron—light—ammonium colimitation of nitrate uptake and phytoplankton growth. *Limnology and Oceanography*, *44*(6), 1436–1446. https://doi.org/10.4319/lo.1999.44.6.1436

Baker, N. R., Harbinson, J., & Kramer, D. M. (2007). Determining the limitations and regulation of photosynthetic energy transduction in leaves. *Plant, Cell & Environment*, *30*(9), 1107–1125. https://doi.org/10.1111/j.1365-3040.2007.01680.x

Baldocchi, D., Falge, E., Gu, L., Olson, R., Hollinger, D., Running, S., et al. (2001). FLUXNET: A new tool to study the temporal and spatial variability of ecosystem–scale carbon dioxide, water vapor, and energy flux densities. *Bulletin of the American Meteorological Society*, *82*(11), 2415–2434. https://doi.org/10.1175/1520-0477(2001)082%3C2415:FANTTS%3E2.3.CO;2

Beer, C., Reichstein, M., Tomelleri, E., Ciais, P., Jung, M., Carvalhais, N., et al. (2010). Terrestrial gross carbon dioxide uptake: Global distribution and covariation with climate. *Science*, *329*(5993), 834–838. https://doi.org/10.1126/science.1184984

Behrenfeld, M. J., & Falkowski, P. G. (1997). Photosynthetic rates derived from satellite-based chlorophyll concentration. *Limnology and Oceanography*, *42*(1), 1–20. https://doi.org/10.2307/2838857

Behrenfeld, M. J., & Milligan, A. J. (2013). Photophysiological expressions of iron stress in phytoplankton. *Annual Review of Marine Science*, *5*(1), 217–246. https://doi.org/10.1146/annurev-marine-121211-172356

Behrenfeld, M. J., Westberry, T. K., Boss, E. S., O'Malley, R. T., Siegel, D. A., Wiggert, J. D., et al. (2009). Satellite-detected fluorescence reveals global physiology of ocean phytoplankton. *Biogeosciences*, *6*(5), 779–794. https://doi.org/10.5194/bg-6-779-2009

Bender, M. L., Dickson, M.-L., & Orchardo, J. (2000). Net and gross production in the Ross Sea as determined by incubation experiments and dissolved O_2 studies. *Deep Sea Research Part II: Topical Studies in Oceanography*, *47*(15–16), 3141–3158. https://doi.org/10.1016/S0967-0645(00)00062-X

Bouteiller, A. L., Leynaert, A., Landry, M. R., Borgne, R. L., Neveux, J., Rodier, M., et al. (2003). Primary production, new production, and growth rate in the equatorial Pacific: Changes from mesotrophic to oligotrophic regime. *Journal of Geophysical Research*, *108*(C12), 8141. https://doi.org/10.1029/2001JC000914

Boyd, P. W., & Ellwood, M. J. (2010). The biogeochemical cycle of iron in the ocean. *Nature Geoscience*, *3*(10), 675–682. https://doi.org/10.1038/ngeo964

Boyle, E. A., Anderson, R. F., Cutter, G. A., Fine, R., Jenkins, W. J., & Saito, M. (2015). Introduction to the U.S. GEOTRACES North Atlantic Transect (GA-03): USGT10 and USGT11 cruises. *Deep Sea Research Part II: Topical Studies in Oceanography*, *116*, 1–5. https://doi.org/10.1016/j.dsr2.2015.02.031

Bricaud, A., Claustre, H., Ras, J., & Oubelkheir, K. (2004). Natural variability of phytoplanktonic absorption in oceanic waters: Influence of the size structure of algal populations. *Journal of Geophysical Research*, *109*, C11010. https://doi.org/10.1029/2004JC002419

Brown, J. H., Gillooly, J. F., Allen, A. P., Savage, V. M., & West, G. B. (2004). Toward a metabolic theory of ecology. *Ecology*, *85*(7), 1771–1789. https://doi.org/10.1890/03-9000

Bruggeman, J., & Kooijman, S. A. L. M. (2007). A biodiversity-inspired approach to aquatic ecosystem modeling. *Limnology and Oceanography*, *52*(4), 1533–1544. https://doi.org/10.4319/lo.2007.52.4.1533

Caperon, J., & Ziemann, D. A. (1976). Synergistic effects of nitrate and ammonium ion on the growth and uptake kinetics of Monochrysis lutheri in continuous culture. *Marine Biology*, *36*(1), 73–84. https://doi.org/10.1007/BF00388430

Capone, D. G., Zehr, J. P., Paerl, H. W., Bergman, B., & Carpenter, E. J. (1997). Trichodesmium, a globally significant marine cyanobacterium. *Science*, *276*(5316), 1221–1229. https://doi.org/10.1126/science.276.5316.1221

Chisholm, S. W. (1992). Phytoplankton size. In P. G. Falkowski, & A. D. Woodhead (Eds.), *Primary productivity and biogeochemical cycles in the sea* (pp. 213–237). New York: Plenum Press.

Clark, J. R., Lenton, T. M., Williams, H. T. P., & Daines, S. J. (2013). Environmental selection and resource allocation determine spatial patterns in picophytoplankton cell size. *Limnology and Oceanography*, *58*(3), 1008–1022. https://doi.org/10.4319/lo.2013.58.3.1008

Daines, S. J., Clark, J. R., & Lenton, T. M. (2014). Multiple environmental controls on phytoplankton growth strategies determine adaptive responses of the N:P ratio. *Ecology Letters*, *17*(4), 414–425. https://doi.org/10.1111/ele.12239

Doney, S. C., Abbott, M. R., Cullen, J. J., Karl, D. M., & Rothstein, L. (2004). From genes to ecosystems: The ocean's new frontier. *Frontiers in Ecology and the Environment*, *2*(9), 457–468. https://doi.org/10.1890/1540-9295(2004)002%5B0457:FGTETO%5D2.0.CO;2

Doney, S. C., Kleypas, J. A., Sarmiento, J. L., & Falkowski, P. G. (2001). The US JGOFS Synthesis and Modeling Project—An introduction. *Deep Sea Research Part II: Topical Studies in Oceanography*, *49*(1–3), 1–20. https://doi.org/10.1016/S0967-0645(01)00092-3

Dortch, Q. (1990). The interaction between ammonium and nitrate uptake in phytoplankton. *Marine Ecology Progress Series*, *61*, 183–201.

Dron, A., Rabouille, S., Claquin, P., Chang, P., Raimbault, V., Talec, A., & Sciandra, A. (2012). Light-dark (12:12 h) quantification of carbohydrate fluxes in *Crocosphaera watsonii*. *ResearchGate*, *68*(68), 43–65. https://doi.org/10.3354/ame%2001600

Dron, A., Rabouille, S., Claquin, P., Le Roy, B., Talec, A., & Sciandra, A. (2012). Light–dark (12:12) cycle of carbon and nitrogen metabolism in *Crocosphaera watsonii* WH8501: Relation to the cell cycle. *Environmental Microbiology*, *14*(4), 967–981. https://doi.org/10.1111/j.1462-2920.2011.02675.x

Dutkiewicz, S., Ward, B. A., Monteiro, F., & Follows, M. J. (2012). Interconnection of nitrogen fixers and iron in the Pacific Ocean: Theory and numerical simulations. *Global Biogeochemical Cycles*, *26*, GB1012. https://doi.org/10.1029/2011GB004039

Eppley, R. W. (1972). Temperature and phytoplankton growth in the sea. *Fishery Bulletin*, *70*(4), 1063–1085.

Eppley, R. W., Rogers, J. N., & McCarthy, J. J. (1969). Half-saturation constants for uptake of nitrate and ammonium by marine phytoplankton1. *Limnology and Oceanography*, *14*(6), 912–920. https://doi.org/10.4319/lo.1969.14.6.0912

Eppley, R. W., Stewart, E., Abbott, M. R., & Heyman, U. (1985). Estimating ocean primary production from satellite chlorophyll. Introduction to regional differences and statistics for the Southern California Bight. *Journal of Plankton Research*, *7*(1), 57–70. https://doi.org/10.1093/plankt/7.1.57

Felcmanová, K., Lukeš, M., Kotabová, E., Lawrenz, E., Halsey, K. H., & Prášil, O. (2017). Carbon use efficiencies and allocation strategies in *Prochlorococcus marinus* strain PCC 9511 during nitrogen-limited growth. *Photosynthesis Research*, *134*(1), 71–82. https://doi.org/10.1007/s11120-017-0418-3

Fernández-Castro, B., Pahlow, M., Mouriño-Carballido, B., Marañón, E., & Oschlies, A. (2016). Optimality-based *Trichodesmium* diazotrophy in the North Atlantic subtropical gyre. *Journal of Plankton Research*, *38*(4), 946–963. https://doi.org/10.1093/plankt/fbw047

Fiksen, Ø., Follows, M. J., & Aksnes, D. L. (2013). Trait-based models of nutrient uptake in microbes extend the Michaelis-Menten framework. *Limnology and Oceanography*, *58*(1), 193–202. https://doi.org/10.4319/lo.2013.58.1.0193

Finkel, Z. V., Beardall, J., Flynn, K. J., Quigg, A., Rees, T. A. V., & Raven, J. A. (2010). Phytoplankton in a changing world: Cell size and elemental stoichiometry. *Journal of Plankton Research*, *32*(1), 119–137. https://doi.org/10.1093/plankt/fbp098

Fisher, N. L., & Halsey, K. H. (2016). Mechanisms that increase the growth efficiency of diatoms in low light. *Photosynthesis Research*, *129*(2), 183–197. https://doi.org/10.1007/s11120-016-0282-6

Flynn, K. J., Marshall, H., & Geider, R. J. (2001). A comparison of two N-irradiance interaction models of phytoplankton growth. *Limnology and Oceanography*, *46*(7), 1794–1802.

Friedrichs, M. A., Carr, M. E., Barber, R. T., Scardi, M., Antoine, D., Armstrong, R. A., et al. (2009). Assessing the uncertainties of model estimates of primary productivity in the tropical Pacific Ocean. *Journal of Marine Systems*, *76*(1–2), 113–133. https://doi.org/10.1016/j.jmarsys.2008.05.010

Galloway, J. N., Schlesinger, W. H., Levy, H., Michaels, A., & Schnoor, J. L. (1995). Nitrogen fixation: Anthropogenic enhancement-environmental response. *Global Biogeochemical Cycles*, *9*(2), 235–252. https://doi.org/10.1029/95GB00158

Geider, R., & La Roche, J. (2002). Redfield revisited: Variability of C:N:P in marine microalgae and its biochemical basis. *European Journal of Phycology*, *37*(1), 1–17. https://doi.org/10.1017/S0967026201003456

Geider, R., MacIntyre, H., & Kana, T. M. (1997). Dynamic model of phytoplankton growth and acclimation: Responses of the balanced growth rate and the chlorophyll a:carbon ratio to light, nutrient-limitation and temperature. *Marine Ecology Progress Series*, *148*, 187–200. https://doi.org/10.3354/meps%20148187

Geider, R. J., MacIntyre, H. L., & Kana, T. M. (1998). A dynamic regulatory model of phytoplanktonic acclimation to light, nutrients, and temperature. *Limnology and Oceanography*, *43*(4), 679–694.

Geider, R. J., Moore, C. M., & Ross, O. N. (2009). The role of cost–benefit analysis in models of phytoplankton growth and acclimation. *Plant Ecology and Diversity*, *2*(2), 165–178. https://doi.org/10.1080/17550870903300949

Grimm, V., Revilla, E., Berger, U., Jeltsch, F., Mooij, W. M., Railsback, S. F., et al. (2005). Pattern-oriented modeling of agent-based complex systems: Lessons from ecology. *Science*, *310*(5750), 987–991. https://doi.org/10.1126/science.1116681

Großkopf, T., & LaRoche, J. (2012). Direct and indirect costs of dinitrogen fixation in *Crocosphaera watsonii* WH8501 and possible implications for the nitrogen cycle. *Aquatic Microbiology*, *3*, 236. https://doi.org/10.3389/fmicb.2012.00236

Gruber, N., & Sarmiento, J. L. (1997). Global patterns of marine nitrogen fixation and denitrification. *Global Biogeochemical Cycles*, *11*(2), 235–266. https://doi.org/10.1029/97GB00077

Halsey, K. H., & Jones, B. M. (2015). Phytoplankton strategies for photosynthetic energy allocation. *Annual Review of Marine Science*, *7*(1), 265–297. https://doi.org/10.1146/annurev-marine-010814-015813

Halsey, K. H., Milligan, A. J., & Behrenfeld, M. J. (2010). Physiological optimization underlies growth rate-independent chlorophyll-specific gross and net primary production. *Photosynthesis Research*, *103*(2), 125–137. https://doi.org/10.1007/s11120-009-9526-z

Halsey, K. H., Milligan, A. J., & Behrenfeld, M. J. (2014). Contrasting strategies of photosynthetic energy utilization drive lifestyle strategies in ecologically important picoeukaryotes. *Metabolites*, *4*(2), 260–280. https://doi.org/10.3390/metabo4020260

Halsey, K. H., O'Malley, R. T., Graff, J. R., Milligan, A. J., & Behrenfeld, M. J. (2013). A common partitioning strategy for photosynthetic products in evolutionarily distinct phytoplankton species. *New Phytologist*, *198*(4), 1030–1038. https://doi.org/10.1111/nph.12209

Halsey, K. H., O'Malley, R. T., Milligan, A. J., & Behrenfeld, M. J. (2012). A common partitioning strategy for photosynthetic products between evolutionarily distinct phytoplankton groups.

Hellweger, F. L., van Sebille, E., & Fredrick, N. D. (2014). Biogeographic patterns in ocean microbes emerge in a neutral agent-based model. *Science*, *345*(6202), 1346–1349. https://doi.org/10.1126/science.1254421

Jacq, V., Ridame, C., L'Helguen, S., Kaczmar, F., & Saliot, A. (2014). Response of the unicellular diazotrophic cyanobacterium *Crocosphaera watsonii* to iron limitation. *PLoS One*, *9*(1), e86749. https://doi.org/10.1371/journal.pone.0086749

Jassby, A. D., & Platt, T. (1976). Mathematical formulation of the relationship between photosynthesis and light for phytoplankton. *Limnology and Oceanography*, *21*(4), 540–547. https://doi.org/10.4319/lo.1976.21.4.0540

Juranek, L. W., & Quay, P. D. (2013). Using triple isotopes of dissolved oxygen to evaluate global marine productivity. *Annual Review of Marine Science*, *5*(1), 503–524. https://doi.org/10.1146/annurev-marine-121211-172430

Kana, T. M. (1992). Relationship between photosynthetic oxygen cycling and carbon assimilation in *Synechococcus* Wh7803 (cyanophyta)1. *Journal of Phycology*, *28*(3), 304–308. https://doi.org/10.1111/j.0022-3646.1992.00304.x

Kana, T. M. (1993). Rapid oxygen cycling in *Trichodesmium thiebautii*. *Limnology and Oceanography*, *38*(1), 18–24.

Klausmeier, C. A., Litchman, E., Daufresne, T., & Levin, S. A. (2004). Optimal nitrogen-to-phosphorus stoichiometry of phytoplankton. *Nature*, *429*(6988), 171–174. https://doi.org/10.1038/nature02454

Kleiber, M. (1932). Body size and metabolism. ENE, 1, E9.

Kleypas, J., & Doney, S. C. (2001). Nutrients, chlorophyll, primary production and related biogeochemical properties in the ocean mixed layer. A compilation of data collected at nine JGOFS Sites (NCAR Technical Report No. TN-447) (p. 55). NCAR.

Knap, A. H., Michaels, A., Close, A. R., Ducklow, H., & Dickson, A. G. (1996). Protocols for the joint global ocean flux study (JGOFS) core measurements. JGOFS, Reprint of the IOC Manuals and Guides No. 29, UNESCO 1994, 19. Retrieved from http://epic.awi.de/17559/1/Kna1996a.pdf

Kostadinov, T. S. (2016). Carbon-based phytoplankton size classes retrieved via ocean color estimates of the particle size distribution. *Ocean Science*, *12*(2), 561.

Kunath, C., Jakob, T., & Wilhelm, C. (2012). Different phycobilin antenna organisations affect the balance between light use and growth rate in the cyanobacterium *Microcystis aeruginosa* and in the cryptophyte *Cryptomonas ovata*. *Photosynthesis Research*, *111*(1–2), 173–183. https://doi.org/10.1007/s11120-011-9715-4

Kustka, A., Sañudo-Wilhelmy, S., Carpenter, E. J., Capone, D. G., & Raven, J. A. (2003). A revised estimate of the iron use efficiency of nitrogen fixation, with special reference to the marine cyanobacterium *Trichodesmium* Spp. (cyanophyta)1. *Journal of Phycology*, *39*(1), 12–25. https://doi.org/10.1046/j.1529-8817.2003.01156.x

Landry, M. R., Ohman, M. D., Goericke, R., Stukel, M. R., & Tsyrklevich, K. (2009). Lagrangian studies of phytoplankton growth and grazing relationships in a coastal upwelling ecosystem off Southern California. *Progress in Oceanography*, *83*(1–4), 208–216. https://doi.org/10.1016/j.pocean.2009.07.026

Laws, E. A., & Bannister, T. T. (1980). Nutrient- and light-limited growth of *Thalassiosira fluviatilis* in continuous culture, with implications for phytoplankton growth in the ocean. *Limnology and Oceanography*, *25*(3), 457–473.

Laws, E. A., Landry, M. R., Barber, R. T., Campbell, L., Dickson, M.-L., & Marra, J. (2000). Carbon cycling in primary production bottle incubations: Inferences from grazing experiments and photosynthetic studies using ^{14}C and ^{18}O in the Arabian Sea. *Deep Sea Research Part II: Topical Studies in Oceanography*, *47*(7–8), 1339–1352. https://doi.org/10.1016/S0967-0645(99)00146-0

Li, B., Karl, D. M., Letelier, R. M., & Church, M. J. (2011). Size-dependent photosynthetic variability in the North Pacific Subtropical Gyre. *Marine Ecology Progress Series*, *440*, 27–40. https://doi.org/10.3354/meps09345

Li, Q. P., Franks, P. J. S., Landry, M. R., Goericke, R., & Taylor, A. G. (2010). Modeling phytoplankton growth rates and chlorophyll to carbon ratios in California coastal and pelagic ecosystems. *Journal of Geophysical Research*, *115*, G04003. https://doi.org/10.1029/2009JG001111

Lindemann, C., Fiksen, Ø., Andersen, K. H., & Aksnes, D. L. (2016). Scaling laws in phytoplankton nutrient uptake affinity. *Marine Ecosystem Ecology*, *3*, 26. https://doi.org/10.3389/fmars.2016.00026

Litchman, E., Klausmeier, C. A., Schofield, O. M., & Falkowski, P. G. (2007). The role of functional traits and trade-offs in structuring phytoplankton communities: Scaling from cellular to ecosystem level. *Ecology Letters*, *10*(12), 1170–1181. https://doi.org/10.1111/j.1461-0248.2007.01117.x

López-Sandoval, D. C., Rodríguez-Ramos, T., Cermeño, P., Sobrino, C., & Marañón, E. (2014). Photosynthesis and respiration in marine phytoplankton: Relationship with cell size, taxonomic affiliation, and growth phase. *Journal of Experimental Marine Biology and Ecology*, *457*, 151–159. https://doi.org/10.1016/j.jembe.2014.04.013

López-Urrutia, Á., Martin, E. S., Harris, R. P., & Irigoien, X. (2006). Scaling the metabolic balance of the oceans. *Proceedings of the National Academy of Sciences of the United States of America*, *103*(23), 8739–8744. https://doi.org/10.1073/pnas.0601137103

Luo, Y.-W., Lima, I. D., Karl, D. M., Deutsch, C. A., & Doney, S. C. (2014). Data-based assessment of environmental controls on global marine nitrogen fixation. *Biogeosciences*, *11*, 691–708. https://doi.org/10.5194/bg-11-691-2014

Luz, B., & Barkan, E. (2000). Assessment of oceanic productivity with the triple-isotope composition of dissolved oxygen. *Science*, *288*(5473), 2028–2031. https://doi.org/10.1126/science.288.5473.2028

Marañón, E., Cermeño, P., López-Sandoval, D. C., Rodríguez-Ramos, T., Sobrino, C., Huete-Ortega, M., et al. (2013). Unimodal size scaling of phytoplankton growth and the size dependence of nutrient uptake and use. *Ecology Letters*, *16*(3), 371–379. https://doi.org/10.1111/ele.12052

Marra, J. (2002). Approaches to the measurement of plankton production. In *Phytoplankton productivity: Carbon assimilation in marine and freshwater ecosystems* (pp. 78–108). Oxford, UK: Blackwell Publ. Ltd.

Marra, J. (2009). Net and gross productivity: Weighing in with ^{14}C. *Aquatic Microbial Ecology*, *56*, 123–131. https://doi.org/10.3354/ame01306

Mawji, E., Schlitzer, R., Dodas, E. M., Abadie, C., Abouchami, W., Anderson, R. F., et al. (2015). The GEOTRACES Intermediate Data Product 2014. *Marine Chemistry*, *177*(1), 1–8. https://doi.org/10.1016/j.marchem.2015.04.005

Menden-Deuer, S., & Lessard, E. J. (2000). Carbon to volume relationships for dinoflagellates, diatoms, and other protist plankton. *Limnology and Oceanography*, *45*(3), 569–579. https://doi.org/10.2307/2670834

Milligan, A. J., Berman-Frank, I., Gerchman, Y., Dismukes, G. C., & Falkowski, P. G. (2007). Light-dependent oxygen consumption in nitrogen-fixing cyanobacteria plays a key role in nitrogenase protection1. *Journal of Phycology*, *43*(5), 845–852. https://doi.org/10.1111/j.1529-8817.2007.00395.x

Moore, C. M., Mills, M. M., Achterberg, E. P., Geider, R. J., LaRoche, J., Lucas, M. I., et al. (2009). Large-scale distribution of Atlantic nitrogen fixation controlled by iron availability. *Nature Geoscience*, *2*(12), 867–871. https://doi.org/10.1038/ngeo667

Moore, J. K., & Doney, S. C. (2007). Iron availability limits the ocean nitrogen inventory stabilizing feedbacks between marine denitrification and nitrogen fixation. *Global Biogeochemical Cycles*, *21*, GB2001. https://doi.org/10.1029/2006GB002762

Moore, R. M., Kienast, M., Fraser, M., Cullen, J. J., Deutsch, C., Dutkiewicz, S., et al. (2014). Extensive hydrogen supersaturations in the western South Atlantic Ocean suggest substantial underestimation of nitrogen fixation. *Journal of Geophysical Research: Oceans*, *119*, 4340–4350. https://doi.org/10.1002/2014JC010017

Morel, A., & Bricaud, A. (1981). Theoretical results concerning light absorption in a discrete medium, and application to specific absorption of phytoplankton. *Deep Sea Research Part A. Oceanographic Research Papers*, *28*(11), 1375–1393. https://doi.org/10.1016/0198-0149(81)90039-X

Morel, A., & Maritorena, S. (2001). Bio-optical properties of oceanic waters: A reappraisal. *Journal of Geophysical Research*, *106*(C4), 7163–7180. https://doi.org/10.1029/2000JC000319

Morel, F. M. M. (1987). Kinetics of nutrient uptake and growth in phytoplankton. *Journal of Phycology*, *23*(1), 137–150. https://doi.org/10.1111/j.0022-3646.1987.00137.x

Morrison, H., Curry, J. A., & Khvorostyanov, V. I. (2005). A new double-moment microphysics parameterization for application in cloud and climate models. Part I: Description. *Journal of the Atmospheric Sciences*, *62*(6), 1665–1677. https://doi.org/10.1175/JAS3446.1

Moseley, J. L. (2002). Adaptation to Fe-deficiency requires remodeling of the photosynthetic apparatus. *The EMBO Journal*, *21*(24), 6709–6720. https://doi.org/10.1093/emboj/cdf666

Mouw, C. B., Hardman-Mountford, N. J., Alvain, S., Bracher, A., Brewin, R. J. W., Bricaud, A., et al. (2017). A consumer's guide to satellite remote sensing of multiple phytoplankton groups in the Global Ocean. *Frontiers in Marine Science*, *4*, 41. https://doi.org/10.3389/fmars.2017.00041

Nicholson, D., Stanley, R. H. R., Barkan, E., Karl, D. M., Luz, B., Quay, P. D., & Doney, S. C. (2012). Evaluating triple oxygen isotope estimates of gross primary production at the Hawaii Ocean Time-series and Bermuda Atlantic Time-series Study sites. *Journal of Geophysical Research*, *117*, C05012. https://doi.org/10.1029/2010JC006856

Pahlow, M., Dietze, H., & Oschlies, A. (2013). Optimality-based model of phytoplankton growth and diazotrophy. *Marine Ecology Progress Series*, *489*, 1–16. https://doi.org/10.3354/meps10449

Pahlow, M., & Oschlies, A. (2009). Chain model of phytoplankton P, N and light colimitation. *Marine Ecology Progress Series*, *376*, 69–83. https://doi.org/10.3354/meps07748

Pahlow, M., & Oschlies, A. (2013). FEATURE ARTICLE: NOTEOptimal allocation backs Droop's cell-quota model. *Marine Ecology Progress Series*, *473*, 1–5. https://doi.org/10.3354/meps10181

Platt, T., Gallegos, C. L., & Harrison, W. G. (1980). Photoinhibition of photosynthesis in natural assemblages of marine phytoplankton. *Journal of Marine Research*, *38*, 687–701.

Quay, P. D., Peacock, C., Björkman, K., & Karl, D. M. (2010). Measuring primary production rates in the ocean: Enigmatic results between incubation and non-incubation methods at Station ALOHA. *Global Biogeochemical Cycles*, *24*, GB3014. https://doi.org/10.1029/2009GB003665

Rabouille, S., de Waal, D. B. V., Matthijs, H. C. P., & Huisman, J. (2014). Nitrogen fixation and respiratory electron transport in the cyanobacterium *Cyanothece* under different light/dark cycles. *FEMS Microbiology Ecology*, *87*(3), 630–638. https://doi.org/10.1111/1574-6941.12251

Rabouille, S., Staal, M., Stal, L. J., & Soetaert, K. (2006). Modeling the dynamic regulation of nitrogen fixation in the cyanobacterium *Trichodesmium* sp. *Applied and Environmental Microbiology*, *72*(5), 3217–3227. https://doi.org/10.1128/AEM.72.5.3217-3227.2006

Raven, J. A., Beardall, J., & Giordano, M. (2014). Energy costs of carbon dioxide concentrating mechanisms in aquatic organisms. *Photosynthesis Research*, *121*(2–3), 111–124. https://doi.org/10.1007/s11120-013-9962-7

Riethman, H. C., & Sherman, L. A. (1988). Purification and characterization of an iron stress-induced chlorophyll-protein from the cyanobacterium *Anacystis nidulans* R2. *Biochimica et Biophysica Acta (BBA) - Bioenergetics*, *935*(2), 141–151. https://doi.org/10.1016/0005-2728(88)90211-3

Rijkenberg, M. J. A., Middag, R., Laan, P., Gerringa, L. J. A., van Aken, H. M., Schoemann, V., et al. (2014). The distribution of dissolved iron in the West Atlantic Ocean. *PLoS One*, *9*(6), e101323. https://doi.org/10.1371/journal.pone.0101323

Rubin, M., Berman-Frank, I., & Shaked, Y. (2011). Dust- and mineral-iron utilization by the marine dinitrogen-fixer *Trichodesmium*. *Nature Geoscience*, *4*(8), 529–534. https://doi.org/10.1038/ngeo1181

Saba, V. S., Friedrichs, M. A. M., Antoine, D., Armstrong, R. A., Asanuma, I., Behrenfeld, M. J., et al. (2011). An evaluation of ocean color model estimates of marine primary productivity in coastal and pelagic regions across the globe. *Biogeosciences*, *8*(2), 489–503. https://doi.org/10.5194/bg-8-489-2011

Saba, V. S., Friedrichs, M. A. M., Carr, M.-E., Antoine, D., Armstrong, R. A., Asanuma, I., et al. (2010). Challenges of modeling depth-integrated marine primary productivity over multiple decades: A case study at BATS and HOT. *Global Biogeochemical Cycles*, *24*, GB3020. https://doi.org/10.1029/2009GB003655

Sakshaug, E., Andresen, K., & Kiefer, D. A. (1989). A steady state description of growth and light absorption in the marine planktonic diatom *Skeletonema costatum*. *Limnology and Oceanography*, *34*(1), 198–205. https://doi.org/10.4319/lo.1989.34.1.0198

Sherman, E., Moore, J. K., Primeau, F., & Tanouye, D. (2016). Temperature influence on phytoplankton community growth rates. *Global Biogeochemical Cycles*, *30*, 550–559. https://doi.org/10.1002/2015GB005272

Shuter, B. (1979). A model of physiological adaptation in unicellular algae. *Journal of Theoretical Biology*, *78*(4), 519–552. https://doi.org/10.1016/0022-5193(79)90189-9

Smith, S. L., Pahlow, M., Merico, A., Acevedo-Trejos, E., Sasai, Y., Yoshikawa, C., et al. (2015). Flexible phytoplankton functional type (FlexPFT) model: Size-scaling of traits and optimal growth. *Journal of Plankton Research*, *38*(4), 977–992. https://doi.org/10.1093/plankt/fbv038

Sohm, J. A., Webb, E. A., & Capone, D. G. (2011). Emerging patterns of marine nitrogen fixation. *Nature Reviews Microbiology*, *9*(7), 499–508. https://doi.org/10.1038/nrmicro2594

Steemann Nielsen, E. (1952). The use of radioactive carbon for measuring organic production in the sea. *Jurnal du Conseil International pour l'Exploration de la Mer*, *18*, 117–140.

Sunda, W. G., & Huntsman, S. A. (1997). Interrelated influence of iron, light and cell size on marine phytoplankton growth. *Nature*, *390*(6658), 389–392. https://doi.org/10.1038/37093

Sunda, W. G., & Huntsman, S. A. (2015). High iron requirement for growth, photosynthesis, and low-light acclimation in the coastal cyanobacterium *Synechococcus bacillaris*. *Microbiological Chemistry and Geomicrobiology*, *6*, 561. https://doi.org/10.3389/fmicb.2015.00561

Talmy, D., Blackford, J., Hardman-Mountford, N., Dumbrell, A. J., & Geider, R. J. (2013). An optimality model of photoadaptation in contrasting aquatic light regimes. *Limnology and Oceanography*, *58*(5), 1802–1818. https://doi.org/10.4319/lo.2013.58.5.1802

Thompson, P. A., Levasseur, M. E., & Harrison, P. J. (1989). Light-limited growth on ammonium vs. nitrate: What is the advantage for marine phytoplankton? *Limnology and Oceanography*, *34*(6), 1014–1024. https://doi.org/10.4319/lo.1989.34.6.1014

Tilman, D. (1982). *Resource competition and community structure*. Princeton, NJ: Princeton University Press.

Twining, B. S., & Baines, S. B. (2013). The trace metal composition of marine phytoplankton. *Annual Review of Marine Science*, *5*(1), 191–215. https://doi.org/10.1146/annurev-marine-121211-172322

Whittaker, S., Bidle, K. D., Kustka, A. B., & Falkowski, P. G. (2011). Quantification of nitrogenase in *Trichodesmium* IMS 101: Implications for iron limitation of nitrogen fixation in the ocean. *Environmental Microbiology Reports*, *3*(1), 54–58. https://doi.org/10.1111/j.1758-2229.2010.00187.x

Yuan-Hui, L., & Gregory, S. (1974). Diffusion of ions in sea water and in deep-sea sediments. *Geochimica et Cosmochimica Acta*, *38*(5), 703–714. https://doi.org/10.1016/0016-7037(74)90145-8

Erratum

In the originally published version of this paper, there were figure labeling errors for Figures 2, 3, and 6. The figures have since been corrected, and this version may be considered the authoritative version.